journal of the American Ceramic Society
Incorporating Advanced Ceramic Materials and Communications

Consolidation and high-temperature strength of monolithic lanthanum hexaboride

Journal:	*Journal of the American Ceramic Society*
Manuscript ID	JACERS-48624.R1
Manuscript Type:	Research Article
Date Submitted by the Author:	n/a
Complete List of Authors:	Demirskyi, Dmytro; Tohoku University Advanced Institute for Materials Research (AIMR), Suzuki, Tohru; National Institute for Materials Science, Research Center for Functional Materials Yoshimi, Kyosuke; Tohoku University, Department of Materials Science and Engineering VASYLKIV, Oleg; National Institute for Materials Science, Research Center for Functional Materials;
Keywords:	grain growth, densification, borides, spark plasma sintering
Author-supplied Keyword: If there is one additional keyword you would like to include that was not on the list, please add it below::	flash sintering

Consolidation and high-temperature strength of monolithic lanthanum hexaboride

D. Demirskyi (a,b,c)†, T.S. Suzuki (b), K. Yoshimi (c), O. Vasylkiv (b)†.

(a) WPI-Advanced Institute for Materials Research (WPI-AIMR), Tohoku University, 2-1-1 Katahira, Aoba-ku, Sendai, 980-8577 Japan

(b) National Institute for Materials Science, 1-2-1 Sengen, Tsukuba, Ibaraki 305-0047, Japan

(c) Department of Materials Science and Engineering, Tohoku University, 6-6-02 Aramaki Aza Aoba, Sendai, 980-8579, Japan

Abstract

In this study we explored the densification, microstructure evolution and high-temperature properties of bulk lanthanum hexaboride. LaB_6 bulks were consolidated using spark-plasma sintering only in the temperature range between 1400 °C and 1700 °C. We adopted flash spark plasma sintering of LaB_6 using a direct current heating without a graphite die. We observed a peculiar grain-size gradient when coarse grains exceeding 300 μm were observed on the top side of the specimen, while the bottom side had a grain size of 15–20 μm. Such large grain were not

† Authors to whom correspondence should be addressed, Dmytro Demirskyi, demirskyi.dmytro.e2@tohoku.ac.jp, Oleg Vasylkiv oleg.vasylkiv@nims.go.jp

observed using SPS at 2000°C, suggesting that these might originate from a local overheating.

Based on the three-point flexural tests, it was observed that the toughness and strength of the LaB_6 were acceptable at room-temperature (3.1±0.2 MPa $m^{1/2}$, 300±20 MPa). However, at 1600 °C, these parameters would decrease to 1.3±0.1 MPa $m^{1/2}$ and 120±40 MPa, respectively.

Keywords: flash sintering; grain growth; densification; borides; spark plasma sintering.

1. Introduction

Rare-earth hexaborides are excellent thermionic electron emitter materials. Among all the binary ceramic compounds ever fabricated, LaB_6 shows the best figure of merit as a thermionic emission material [1–4]. LaB_6 was determined to have many advantageous properties, including a low electron work function and good chemical resistance [1,4,5]. The melting-point is high, generally exceeding 2200 C (~2210 °C is the lowest reported [4], as the melting point may depend on impurities and is sensitive to the B to La ratio) [1–3]. Based on this combination of properties, LaB_6 plays an important role in several industries, while its composites with SiC have the potential for novel applications in harvesting of solar energy [6].

Like other hexaborides, a majority of the properties come from the crystallographic structure. LaB_6 has an interpenetrating simple cubic structure in which the La atom sits in the center while boron octahedrons occupy the corners of the unit cell [1,2]. In this configuration, covalent bonds between the boron atoms provide the hardness [1,7] and stability of the structure at elevated temperatures, while the free electrons of the lanthanum atoms are responsible for its hot-emission properties.

Other noticeable features of the lanthanum hexaboride are a relatively low specific density (4.72 g/cm^3) similar to TiB_2 and its ability for the near-infrared absorption which is useful for special coatings.

As a structural material, only a few studies have reported the strength or toughness at room temperature [8–10]. Zhou et al. [11] reported that the local doping of LaB_6 with Sm may lead to a strength increase. Nonetheless, the high-temperature strength data were confined to the LaB_6-based eutectic composites with transition metal diborides [12,13]. In these studies, it was shown that the LaB_6-based ceramic composites containing ZrB_2 or TiB_2 fibrils will show an increase in their flexural strength up to 1600 °C. This was explained by the activation of the plastic deformation in the eutectic system, however, such phenomenon for regular composites should lead to a decrease in their strength. In this regard, it is important to reevaluate the possibility of lanthanum hexaboride being used as a high-

temperature structural material because only a selected number of monolithic ceramic compounds may experience a strength increase at 1600 °C.

In addition, it is important to note that a number of recent reports about the processing of LaB_6 or other hexaboride would involve spark plasma sintering [8,11,14]. This method is known for its ability to achieve the near-theoretical density in a matter of minutes, rather than hours using a 5–10°C/min heating or cooling rate [10]. However, the specifics on the densification kinetics are rarely reported [11,14]. The authors failed to find any reports about the analysis of the densification process for LaB_6, hence, it was suggested that this study focus on the processing of lanthanum hexaboride. A step forward from the SPS would be to densify LaB_6 in the flash mode, i.e., an electrical current directly passes through the material without the use of a graphite die. LaB_6 is known to have an increase in electrical resistivity from 20 μΩ cm at room-temperature to 120 μΩ cm at 1600°C [15]. Furthermore, the resistivity at 2000 °C can be as high as 350 μΩ cm for LaB_6 with a relative density of 60% of the theoretical density (TD) [16]. As a cathode material, when heated to above 1200°C, the lanthanum hexaboride will emit its own electrons, making it a *de facto* local plasma source. Macroscale devices of LaB_6 operating in helium were recently proposed as a plasma source for the next generation of tokamaks [17]. The local electron cloud emitted between grains on a microscale may promote the

material's ability to locally self-heat itself. These are precursors that share some similarities with the regular flash sintering phenomenon [18].

In the present study, the effect of processing on the microstructure, toughness, strength, and the performance at high-temperatures of LaB_6 fabricated by SPS was examined. We expect that the high-temperature strength can result in a strength increase as suggested for the LaB_6-based ceramic composites [12,13], which is the focus of this paper. Thus, the purpose of this study is to report the detailed processing conditions, microstructure evaluation and structure–property relationships of the LaB_6 ceramics processed by SPS. For the latter purpose, we used conventional SPS with a graphite die to evaluate the densification kinetics, while die-free or direct SPS in the 'flash' regime [19–21] was explored as a potential rapid method for producing bulk lanthanum hexaboride.

2 Materials and Methods

Commercially-available LaB_6 (Lot #64647, Mitsuwa Chemical Co., Ltd. Japan) powder was used as the starting material. LaB_6 powder had a mean particle size of 5±1 μm. The concentration of the secondary elements in the LaB_6 was as follows: Fe ≤ 90 ppm, Ce ≤ 50 ppm, C≤ 0.5 wt.%, N ≤ 0.5 wt.%, and O ≤0.5 wt.%. Boron content was within 32.8±0.5 wt.%. The received untreated powder was used for consolidation by the SPS using the 'Dr. Sinter' 1050 (Sumitomo, Japan) unit with a

25-mm or 30-mm die. For all the specimens we used an inner Ta-foil and outer graphite foil configuration, in which the Ta-foil would be in direct contact with the powder. From the top of the specimen the Ta-foil would be followed by the graphite circle, and to distinguish the bottom side, Nb+graphite configuration was used. These steps were made to minimize the diffusion of carbon [22,23] into the LaB_6 or to assist the pre-heating during the flash spark plasma sintering (FSPS).

Green specimens for the FSPS runs were consolidated at 1000°C using a 5-min dwell and pressure of 40 MPa. 50 °C/min heating and cooling rates were used. These specimens had a relative density of 48 to 52 % of the TD.

The schedule for the lanthanum hexaboride isothermal kinetics can be summarized as follows: the LaB_6 specimens prepared in this study had four major steps: (1) heating to 900 °C in four minutes followed by (2) a 50 °C/min heating to the densification temperature. A dwell up to 20 min was used. The final step included cooling to 600 °C at the rate of 40°C/min. The pressure of 40, 60 or 80 MPa was maintained during the consolidation and cooling stages. Argon gas at the flow rate of 2 L/min was used. Based on the previous studies [8–10], the densification temperature of the LaB_6 was selected between 1200 °C and 1700 °C. In [8], it was suggested that 5 min dwell at 1200 °C should be enough to achieve full density for nanocrystalline LaB_6. While in [9], pressureless sintering at 1950 °C/2h resulted in

only 85.1% of the TD, while hot-pressing at 1950°C/2h resulted in 99.9 % of the TD.

In the case of the FSPS, after cooling, the green specimens pre-consolidated at 1000 °C were removed from the graphite die and subjected to a mold-free [19–21] FSPS consolidation. This step consisted of wrapping the pre-consolidated LaB_6 specimens with additional graphite foils and placed in the setup described in ref [19]. The Sumitomo unit was operated in the current control mode, thus a current limit of 2000 to 3000 A was selected based on previous FSPS runs to reach the temperature of 1600 °C.

The temperature during the FSPS experiments was determined by a side pyrometer focused on the side of the graphite felt using an emissivity of 0.90. In order to minimize any errors associated with the emissivity during the temperature measurements, a top layer of graphite foil was painted with a graphite paint that originated from the crushed die used for the SPS. Because the graphite felt is a thermal insulator, a tolerance for the accuracy of the temperature measurement was considered as ±10 °C. Based on our previous studies of the densification kinetics using FSPS one can presume that the sample temperature was at least 100 °C hotter than the probed one [21]. For all the FSPS experiments, a constant uniaxial pressure of 18 MPa was applied. The apparatus was operated in the constant current control mode. In this case, a typical heating profile would always have a dome-like top, and

after reaching a peak temperature, despite a constant current and voltage, the temperature of the specimen would remain constant or decrease. After shutting down the unit, the specimens usually cooled down to 570–600°C withing 60 to 90 s. The FSPS experiments were performed in argon gas at the flow rate of 2 L/min.

An X-ray diffraction (XRD) analysis (D8 Advance, Bruker, Karlsruhe, Germany) was performed on the polished surfaces of the bars of the flexural tests using Cu-Kα radiation. The intensity data were collected over the 2θ range of 20°–145° in steps of 0.02–0.05° using a sampling time of 5 s for each step. The software used for refinement was TOPAS (TOPAS Ver. 4.2, Bruker AXS, Germany).

The structural characteristics of the lanthanum hexaboride ceramics were studied by scanning electron microscopy (SEM, JCM-6000, JEOL) with secondary electrons (SE) or backscattered electrons (BSE mode).

The three-point flexural strength was determined using rectangular blocks (2 mm×2 mm×25 mm, 2 mm×2.5 mm×25 mm) and the strength testing equipment that was previously described in detail [24]. A span of 16 mm was used. The fracture toughness of the ceramics was evaluated by the specimen bending testing which contained a single edge through-thickness notch (2 × 4 × 25 mm, notch width 90 μm, depth 0.4–0.6 mm, a/W <0.15) following ASTM C1421-16. At least three tests with loading rates of 0.05 and 0.5 mm/min were performed. Eight tests were conducted at room temperature and six specimens were tested at elevated

temperatures. For the fracture toughness, the high temperature tests were performed at 1000 °C, 1200 °C and 1600 °C. Tests below 1800 °C were performed at the loading rate of 0.5 mm/min. Tests at elevated temperatures were performed in argon [24], and the loading rate of 3 mm/min was used at 1800 °C or 2000 °C. We evaluated the elastic modulus (Ef) for the tests from the linear portion of the load-displacement curve using the procedure described in ASTM E111–04. Within this study, the compressive load during flexural tests was applied parallel to the pressing direction used in the SPS/FSPS procedure.

The toughness was tested in the same direction as the applied pressure during the SPS consolidation. Details of the testing configuration and the notch profile were presented in ref. [25]. In the case of the FSPSed specimens, a notch was made on the top side of the specimen. This side was facing the electrode providing current for the sintering process.

The hardness was determined by an MMT-7 Vickers hardness tester (Matsuzawa MMT-7; Matsuzawa SEIKI Co., Ltd., Tokyo, Japan) using loads of 9.8 N and 98 N with a dwell time of 15 s following the standard procedure (ASTM C 1327–15). Hardness measurements were performed on the surface polished down to 0.1 μm diamond polishing paste.

3. Results and discussion

3.1. Isothermal sintering of LaB_6

Figure 1 shows the effect of the dwell time and temperature on the relative density at the constant pressures of 40, 60 and 80 MPa. The common observation can be made that when using a temperature of 1600 °C or 1700 °C density close to the theoretical density can be obtained within a relatively short dwell. Because there are no data for the diffusivity or densification kinetics of this compound, and, crucially, no data on creep mechanism(s) in LaB_6, we decided to use an approach proposed by Murray et al. for analysis of the densification kinetics [26,27]. Originally, the approach was developed on the basis of the theoretical model of a viscous flow mechanism, but was successfully used for a number of compounds [27–30]. The densification process of an amorphous powder body under load should obey the following relationship [26,31]:

$$dD/dt = 4P / 4\eta (1 - D)$$

leading to

$$\ln (1 - D) = -3P/ 4\eta t + \ln (1 - Di)$$

where D is the relative density (i.e., $D = \rho/\rho th$, ρ is the measured density, and ρth is the theoretical density (XRD density)), Di is the initial relative density, η is the viscosity in Pa·s, P is the applied pressure in N/m^2 and t is the time.

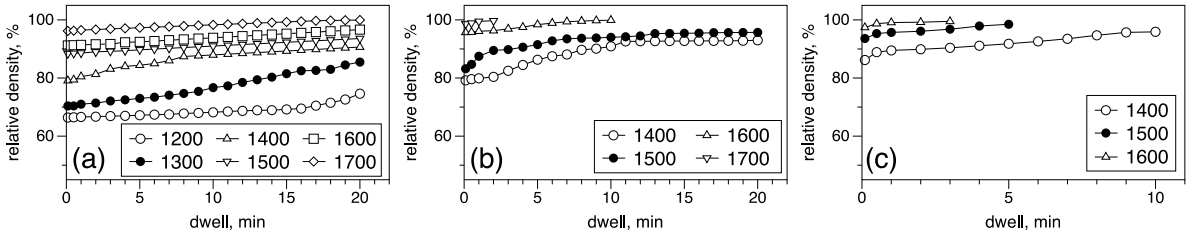

Figure 1. Effect of temperature and dwell on relative density the LaB_6 using the constant pressure of (a) 40 MPa, (b) 60 MPa, and (c) 80 MPa.

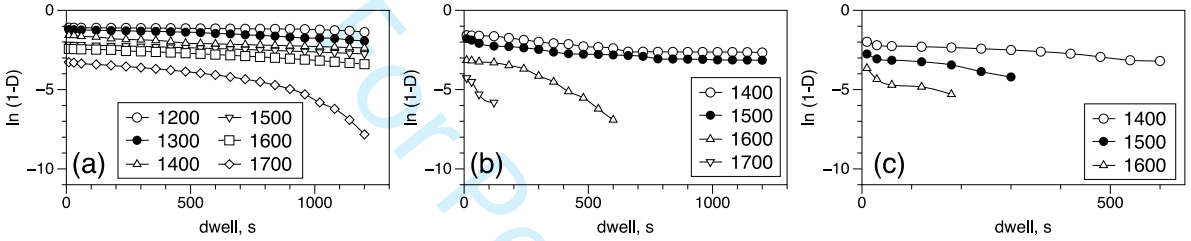

Figure 2. Relationship between logarithm of porosity and time for LaB_6 compacts SPSed at various temperatures using the constant pressure of (a) 40 MPa, (b) 60 MPa, and (c) 80 MPa.

Based on this model, the effective viscosity of the powder body can be evaluated using a plot of ln (1 – D) vs time. Such plots are presented in **Fig. 2**. Because we used different pressures, the viscosities can be evaluated for every pressure. Such an analysis would yield the activation energy for diffusion of 105±40 kJ/mol, 254±19 kJ/mol, or 192±10 kJ/mol for 40 MPa, 60 MPa, and 80 MPa, respectively. Despite a slight scatter between the values, one notes that within a close approximation based on the three pressures, the activation energy of 150±30 kJ/mol (**Fig. 3**) may be used

to describe the densification process of lanthanum hexaboride. For reference, the molar enthalpy of formation of LaB_6 was estimated to be 527 kJ/mol in [1,2], or 400±19 kJ/mol in [32]. Activation energy for the evaporation of the lanthanum hexaboride was estimated to be 698.7 kJ/mol for the temperature range 1730–1910 °C [1]. As noted by Lafferty [4], this process is directly related to diffusion of La via migration in the boron sublattice.

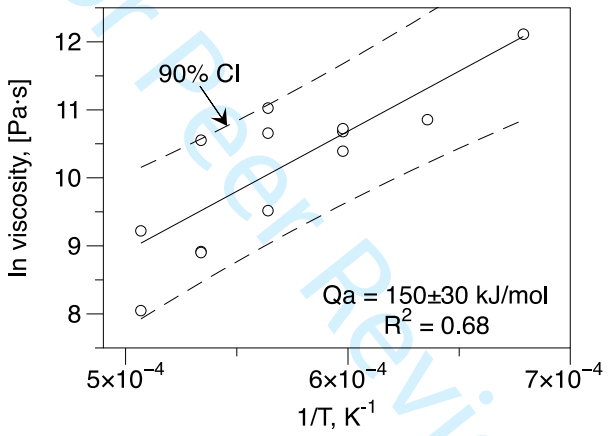

Figure 3. Arrhenius dependence of logarithm of viscosity evaluated for LaB_6 during spark plasma sintering using the constant pressures of 40, 60, and 80 MPa.

In terms of the level of actual values of the viscosities predicted by this approach, it is observed in **Fig. 4** [33–35] that the powder body has not reached an amorphous (liquid-like) state as do most metals while approaching their melting points (see La or Ta) that would show a viscosity similar to milk at room temperature.

At the same time we noticed that processing at relatively low temperatures using SPS may be beneficial to the grain size. **Figure 5** shows a summary for the grain size for the various SPS runs. The largest grain size (33.0±4.2 μm) was observed for the 10 min run at 1600°C at the pressure of 60 MPa.

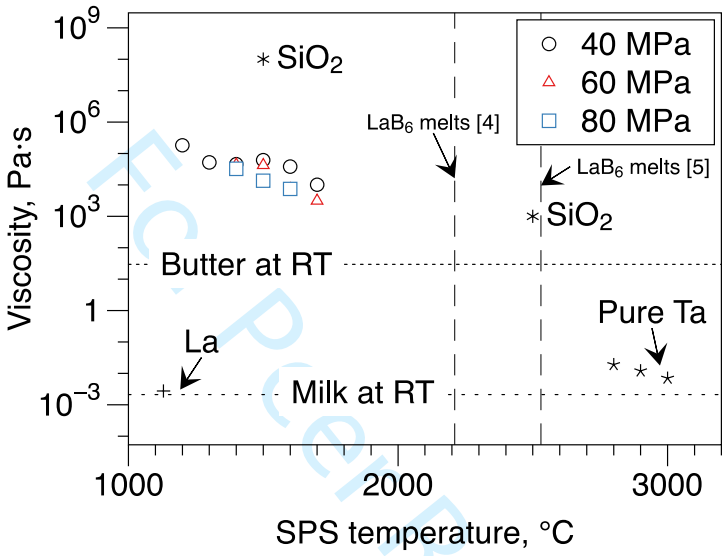

Figure 4. Effect of temperature on the evaluated viscosity of the LaB_6 using different pressures.

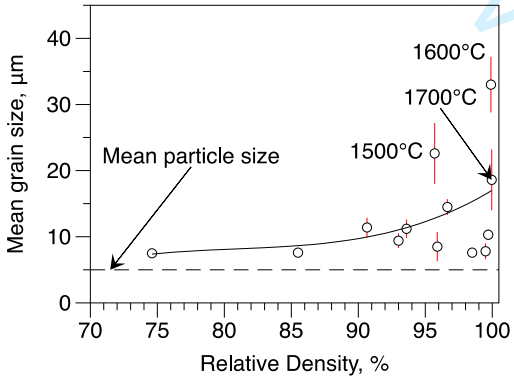

Figure 5. Grain size as a function of the relative density during isothermal dwell runs using spark plasma sintering. We present the temperature for the isothermal dwell in the case of extremely coarse grains.

3.2. Flash spark plasma sintering of LaB_6

In order to attempt to preserve the processing time or minimize the grain growth [18], we attempted to perform flash spark plasma sintering experiments on the lanthanum hexaboride. Multiple runs were performed using pre-consolidated specimens at 1000°C/5 min/40 MPa (48–52 % TD, 5±1 μm mean grain size). The approach described in depth in [19–21] was used. In short, the flash SPS was performed on the specimens without the graphite die using thick top and bottom graphite sheets in order to minimize any contact between SPS press and specimen. The fixed load of 18 MPa was used for the flash SPS runs. The pre-consolidated powder specimen was encapsulated in Ta foil / Graphite foil combination, so that tantalum carbide would be formed as a protective medium for the LaB_6. The outer layer of the graphite foil was painted with the graphite paint (made from the crushed SPS die) to ensure that the reading of the pyrometer would be identical during in the FSPS or SPS. In order to distinguish the top side of the specimen from the bottom side, as a rule, we covered the top of the specimen with Ta+Graphite foil, while the bottom was covered with the Nb+Graphite foil combination.

Once the SPS process was initiated, an incubation period would be required in order to preheat the graphite felt, or directly initiate the current flow thought the specimen if the specimen becomes conductive. Unlike zirconia, SiC or HfB_2, this preheating time was at most 20 seconds. The electrical and emissive properties of LaB_6 are well studied [15], and in some reports, the electrical resistivity is directly proportional to the temperature within a 900–1600 °C range. Thus, once the lower end of this temperature is being reached the specimen can self-heat itself due to the ohmic loses [36].

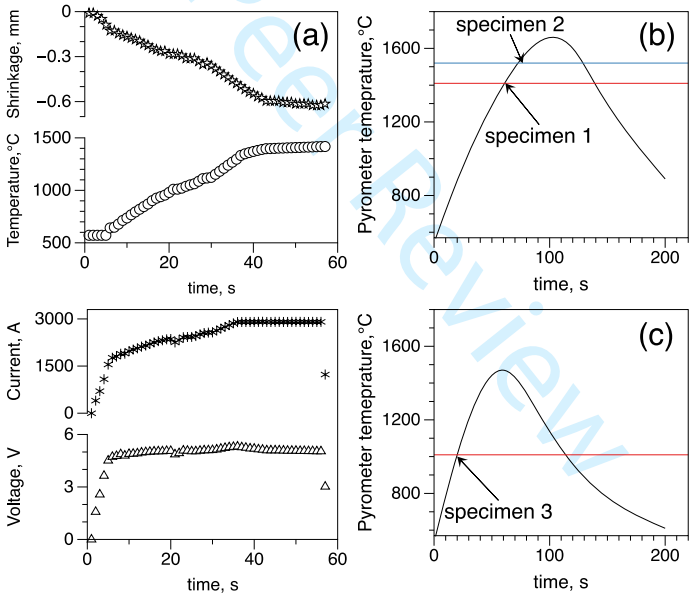

Figure 6. Variation in shrinkage, temperature, current and voltage during flash SPS of LaB_6. Note the quasi-linear dependance between the temperature and current. The maximum current was fixed at (a) 3000 A, (b) 2000 A, and (c) 2700 A. The

horizontal lines are for the reference specimens stopped during heating that were used to understand the microstructure evolution.

In order to understand the densification process during the flash SPS, we stopped the runs at selected temperatures **(Fig. 6)**. **Figure 7** shows the cross-section of specimen #3 after the flash SPS at 1300±20 °C. First, the tantalum carbide layer marks the top of the specimen, and, hence, the current flow is from the bottom to top. Second, there is no reaction between the TaC and LaB_6. Third, the specimen is being quickly densified only by ~500 μm inside the pre-consolidated specimen, while the mean grain size remained identical to the green specimen (5±1 μm).

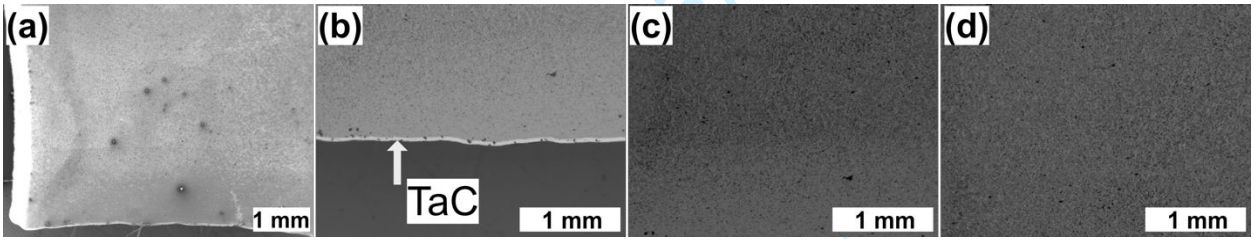

Figure 7. Representative microstructures of lanthanum hexaboride consolidated using flash SPS at different locations on the specimen. Flash SPS process was stopped after reaching ~1300±20°C (see specimen 3 in **Fig. 6 (c)**). Current flow is from the bottom to top. Images are taken in the BSE mode. The 20–25 μm thick tantalum carbide layer that originated from the green-specimen processing can be seen as a white continuous strip. No reaction between Ta or TaC with LaB_6 was

noticed during processing. The thickness of the green specimen was approximately 10 mm, and at an ~500 μm distance from the top surface a more dense microstructure was observed. The mean grain size was unchanged at 5±1 μm. The black areas are pores or dirt introduced during polishing of the specimen.

With an increase in the flash temperature, **Figure 8**, a peculiar grain-size evolution is noted while observing the specimen. First, there is a distinct coarse grain area without any observed porosity (see **Fig. 8 (b,c)**). Second, it was noted that the size and the shape of the grains are completely random, although, in all cases, exceeding 100 μm. In some reports about hexaborides [8,11,14], there are distinctive findings that the cubic-like grains can be preserved even in bulk specimens. There are then areas of void-like cavities, which may originate due to the grain rearrangement during fast densification. As the volume is still somehow constrained, the particle accommodation, such as formation of a brick-style wall can be expected. Finally, after reaching ~ 3 mm inside the specimen the grain size and porosity become constant. There is a slight increase in the grain size (9±2 μm), if one completely removes the 3-mm layer by polishing, and the relative density of the specimen exceeded 98 % of the TD. These suggested that some of the black areas observed in (j) are grain-pull outs and not the pores.

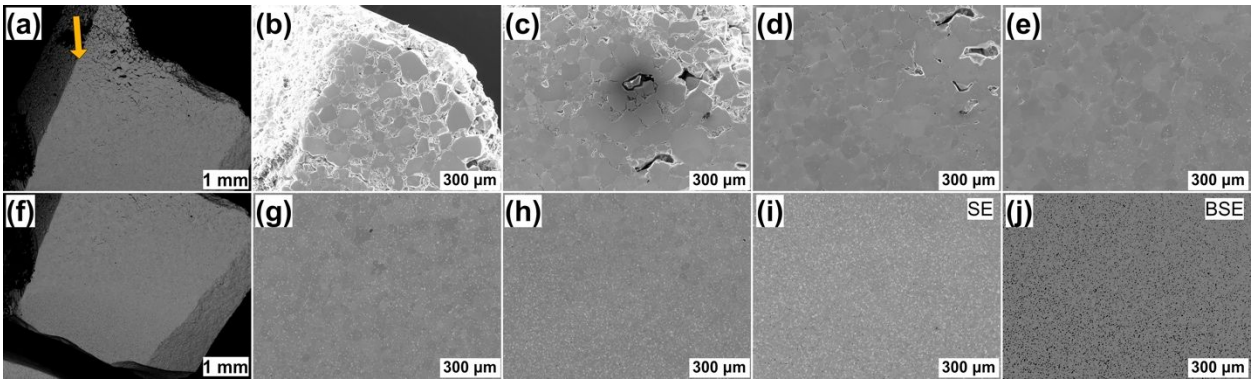

Figure 8. Representative microstructures of lanthanum hexaboride consolidated using flash SPS at different locations on the specimen. The flash SPS process was stopped after reaching ~1410±10°C. Current flow is from the top to bottom as indicated by the arrow in (a). Macroscopic images are taken in the BSE mode. The thickness of the green specimen was 8 mm. The black areas in (j) are pores or pull-outs introduced during polishing of the specimen.

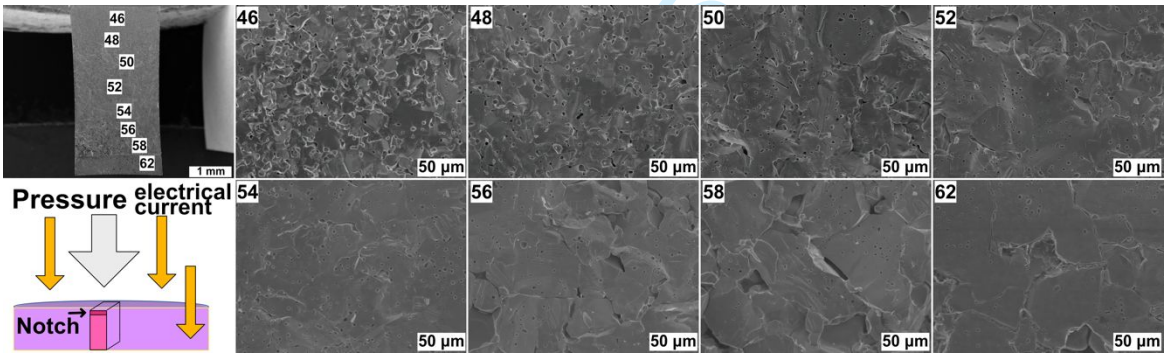

Figure 9. Representative microstructures of lanthanum hexaboride consolidated using flash SPS at 1480±10°C at different locations on the specimen. Internal SEM numbering was used. This is a half-bar after the flexural test to determine the fracture toughness at room temperature.

A further increase in the temperature leads to a dense specimen, and the large-sized area becomes localized. **Figure 9** shows a specimen after the room-temperature fracture toughness test that originated from the 7-mm thick green specimen. The flash SPS was stopped at 1480±5°C. After cooling the specimen was crack-free, and only ~50 μm layers from the top and bottom were removed prior to fabrication of the specimen for the fracture toughness test. **Figure 10** summarizes the porosity using ImageJ [36] and analyzing the spherical pores as well as grain size for different areas of the bar after the toughness tests. One can assume that the area for the extremely coarse grains is limited by the top 1 mm of the specimen, while moving further inside, the flashed specimen grain size equalizes at 30 μm within a 3 mm depth. The pore size remained rather constant, and in the bottom of the specimen the total porosity was less than 0.6 %.

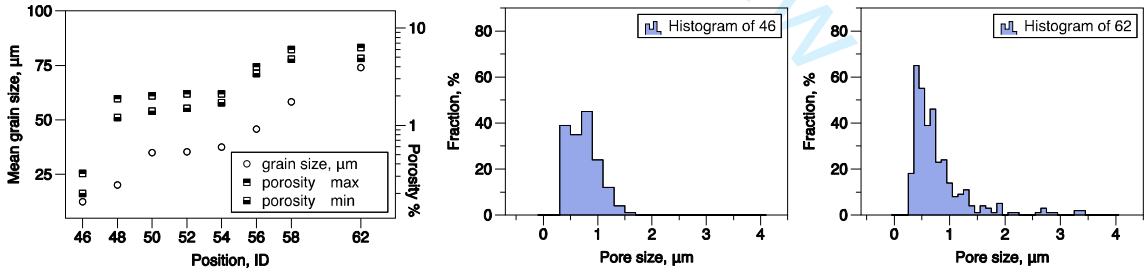

Figure 10. Mean grain size and total porosity for lanthanum hexaboride consolidated using flash SPS at different locations on the specimen. Numbers are the same as in **Fig 9**. (b) and (c) show the histograms for the pore-size distribution at different ends of the specimen.

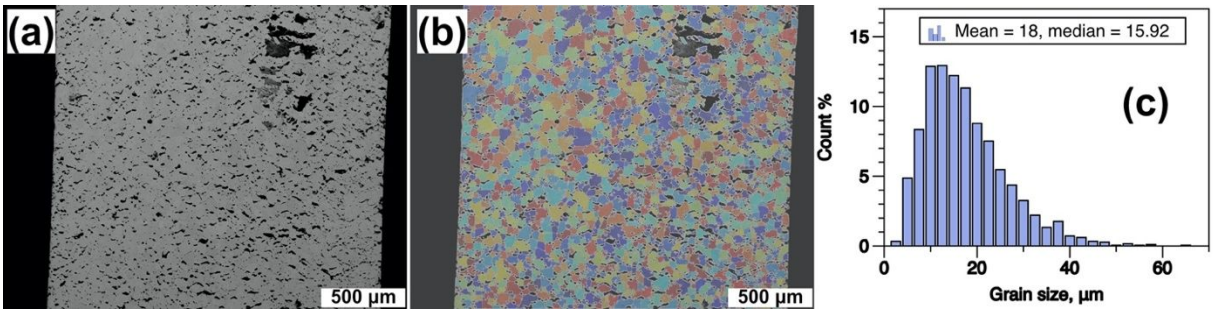

Figure 11. Representative microstructure of lanthanum hexaboride consolidated using flash SPS at ~1500±10°C. Current flow is from the top to bottom. The thickness of the green specimen was 5 mm. (a) image is taken in the BSE mode. (b) image shows the algorithm for evaluation of the grain size using a self-learning engine. (c) provides a grain size distribution for the specimen. The black areas in (a) and (b) are grain pullouts during polishing or voids associated with fast grain-growth and related accommodation in the enclosed volume.

Figure 11 shows the top surface of the bulk LaB_6 using a thinner green specimen (5 mm) and flash SPS was stopped at 1500±10°C. The current flow was from the top to bottom. One can see that similar to **Fig. 9** there were a lot of pull-out voids, while the mean grain size remained below 20 µm. Finally, after optimization of the processing, we were able to produce a fine-grained specimen using the flash SPS. **Figure 12** shows the typical microstructure for such an attempt. As expected, the X-ray diffraction results showed (**Fig. 13**) that only LaB_6 peaks were detected. The

lattice parameter remained constant (a = 4.156 Å) for the powder, SPSed or FSPSed specimens.

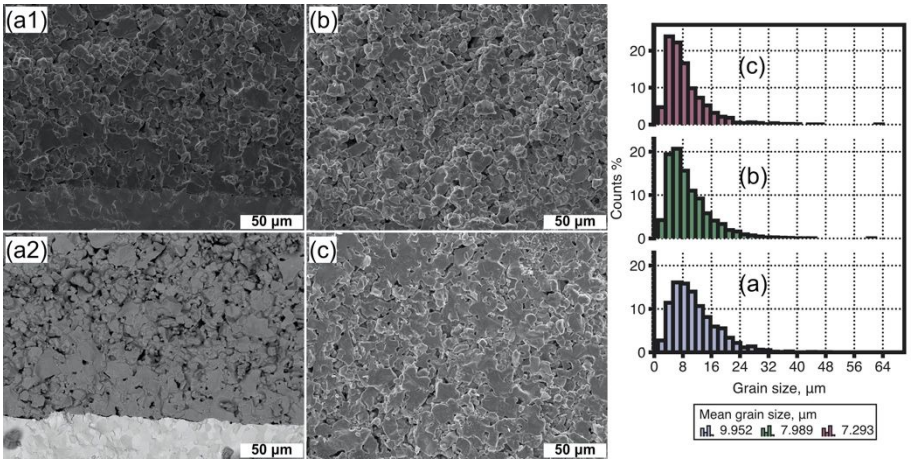

Figure 12. Representative microstructures of lanthanum hexaboride consolidated using flash SPS at ~1500±20°C. Current flow is from the bottom to top. The thickness of the green specimen was 6 mm. (a2) image is taken in the BSE mode. The 30-µm thick tantalum carbide foil originated from the green-specimen processing can be seen as a white continuous strip in (a2). Right side shows grain size distribution for SEM images observed 300 µm from each other. Relative density of the specimen was 98.7±0.2% of the theoretical density.

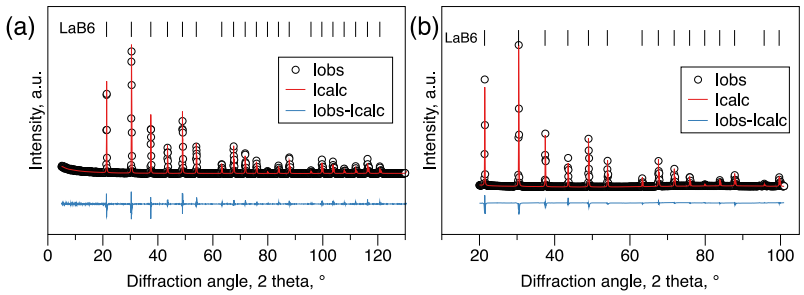

Figure 13. Diffraction pattern of the lanthanum hexaboride specimen (a) before FSPS, and (b) after FSPS.

Structure evolution during the flash SPS might suggest that lanthanum hexaboride will instantly densify as a result of the direct heating. The specimen quickly (instantly) densifies, but as we reach a temperature saturation point during the FSPS, overheating and grain growth occurs. The kinetics of the grain growth cannot be understood at the moment as it may be directly connected to the temperature, and temperature propagation in a short time slot which is limited (or constrained) by thermal diffusion of the LaB_6. As already noted, when heated, the LaB_6 may act as a source of electrons or plasma discharges. Due to a difference in resistivity of the porous and bulk LaB_6 [16], local overheating is quite plausible. Using the approach of Raitchenko [35] described in [37] for YSZ, one can estimate that for LaB_6 at 1600 °C a maximum temperature gradient should lie within 300–350 °C. Data regarding the resistivity, thermal capacity, and specific heat capacity are taken from [16,5,38]. Here it is important to stress the short processing time during the FSPS. Note that the melting was not observed during any of the FSPS runs. During the microstructure evaluation, we did not encounter any grains that had resemblance to the solution-precipitation process characteristic for the liquid phase sintering. On the contrary, a large number of pores that were entrapped inside the grains indicate that

gases were entrapped during ultra-fast consolidation. Using our previous estimate for a 100 °C [21] minimum difference between the probe temperature at the graphite foil and sample temperature, one can presume that 1500°C can be at most viewed at 1950°C. Furthermore, we did not observe such coarse grains during the regular SPS (**Fig. 14**), while specially performed runs at 2000 °C without a dwell would result in the grain sizes of 40–70 μm as presented in (**Fig. 15**). We also observed that for specimens prepared at 2000 °C by SPS, the pores were predominantly located near or at the grain-boundaries, and their size was ~1 μm. One may also notice that the specimens after heating at 2000 °C were severely cracked either at the specimen center (**Fig. 15 (a)**) or at the edge (**Fig. 15 (b)**). These features were not observed in **Figure 8**, suggesting that the coarse grains can be obtained by instant overheating. Another peculiarity of the top side in **Fig. 8** is that the coarse and less-coarse grains are well accommodated like a brick-wall prototype. As pores are absent for such coarse grains, we cannot hypothesize the exact mechanism of local densification/grain growth, thus further studies are required.

Lafferty [4] summarized the key points on the use of LaB_6 as a cathode material at elevated temperatures regarding the diffusion processes. Because the surface is significantly involved, it was summarized that lanthanum on the LaB_6 surface is replaced, and a vacancy occurs at a faster rate compared to the ability of the lanthanum to evaporate from the LaB_6. Obviously, the evaporation rate, as well as

the emissivity, have different rates from different crystallographic orientations on the surfaces [1–3,39]. According to Lafferty [4] the average lifetime of a lanthanum atom on the LaB_6 surface is five minutes at 1500 °C, while the average replacement time for this atom is only six seconds. With an increase in the temperature and time, the emission would decrease due to the inadequate rates of the alkaline-earth metals through the boron framework. At the temperature of 1200 °C, the emission cannot be instantly activated, due to the slow diffusion of La in the boron framework. Based on these observations, one can hypothesize that the shape of the heating curve during the flash experiments should be at some point connected to the diffusivity of La in the boron framework, since it is a common observation that hexaborides would essentially have a local non-stoichiometry as LaB_{6-x} [1]. These LaB_{6-x} crystals would have a deviation in the lattice parameter as well as in the color ranging from violet to dark blue. The polished surface presented in **Fig. 8** had an even, non-changing mild violet color or light purple color (color gradation depended on the light source, under the natural lighting conditions, the color was similar to that used on the Tohoku University logo), and the same was true for the outer surface of the bar presented in **Fig. 9**. The macroscopic observations do not directly imply that the chemistry of the grains, would not be different from another taking into account the observations made for the cathodes [4]. Note that creep deformation, the heating process or the diffusion is always non homogeneous. For this reason, in practical

applications, the majority of the processes is slow. Hence, one should consider the artifacts of the gradient in the grain-size (**Figs. 8, 9**) as the incomplete process or a stage of the ongoing process, as similar observation were made for HfB_2, where the coarse grains were imbedded into the fine-grained matrix [21]. Strangely enough, this structure does not seem to have a direct impact on the strength or toughness at room-temperature. The bar presented in **Fig. 9** showed an adequate toughness (3.05 MPa $m^{1/2}$) at room-temperature. With that in mind, one can presume that if the appearance of coarse grains cannot be controlled during the FSPS or similar high-rate heating techniques, this part of the specimen can be just removed by polishing.

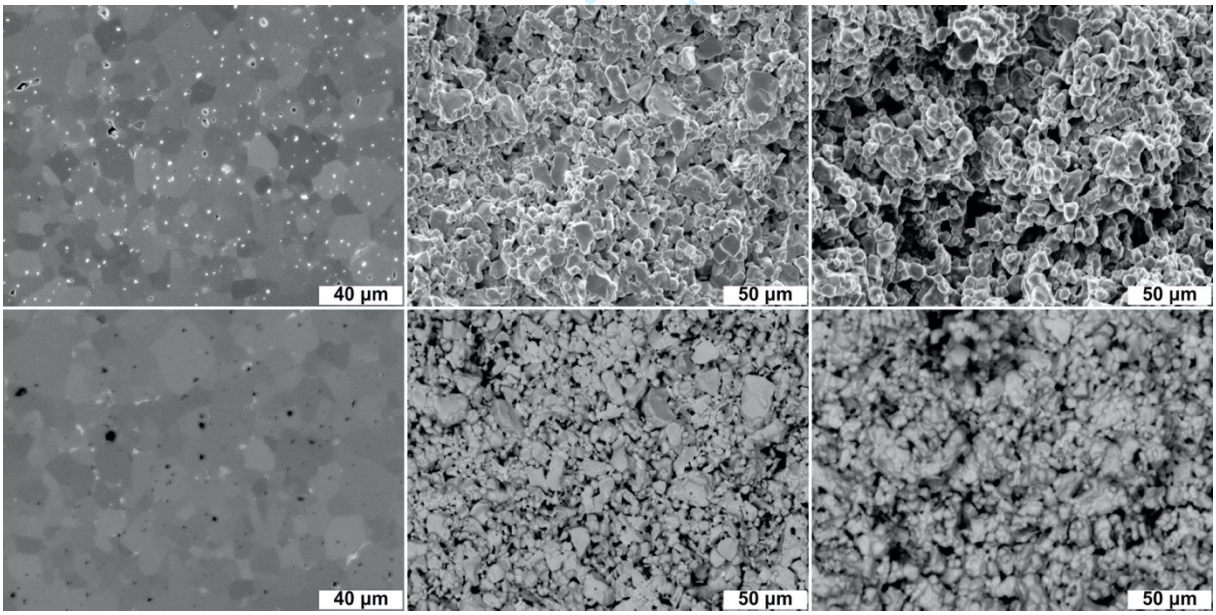

Figure 14. Representative microstructures of lanthanum hexaboride consolidated using SPS at 1700 °C and pressure of 40 MPa. (a,d) polished surface, black areas in

(d) are pores and pull-out grains. (b,e) and (c,f) are fractured at 1600 °C and 1800 °C, respectively.

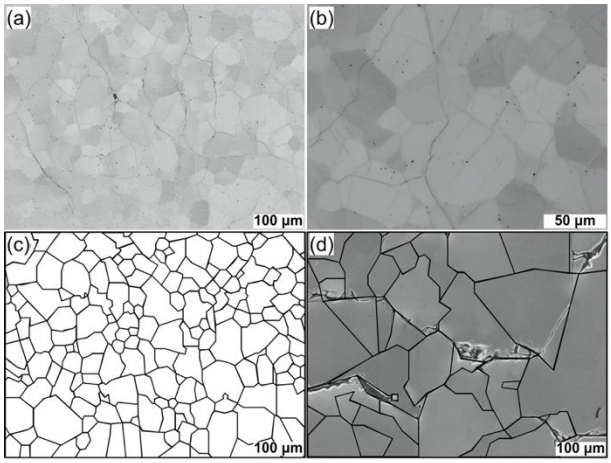

Figure 15. Representative microstructures of lanthanum hexaboride consolidated using SPS at 2000 °C and pressure of 50 MPa. Specimens were heated and cooled at the rate of 100°C/min. Dwell was not used. (a) is for the specimen center, while (b) was observed at the specimen edge. In both cases, the top polished surface was used. Images are taken in the BSE mode. (c) and (d) show typical grain-boundary shape using the self-learning engine. (c) for the SPS at 2000°C using (a); and (d) for the FSPS (**Fig. 8 (d)**) using identical magnification.

3.3. Mechanical properties of LaB_6 bulks

The hardness of the LaB_6 using a 96 N load was 16.3±0.4 GPa. At the lower load of 9.6 N, the hardness data showed a more profound deviation of 17.2±1.8 GPa,

however, the grain size or density had a weak or no effect on the hardness. Sonber et al. reported a hardness of 20.34 ± 1 GPa using a 100g-foce load [9]. Otani et al. reported the room temperature hardness of LaB_6 to be around 20 GPa using a 200g-force load [40]. In [40], the hardness decreased with an increase in the temperature. Zhou et al. reported the hardness of LaB_6 as 22.3 GPa using a 1 kg load [9]. Loboda et al. reported the microhardness (1.5 N load) and nano-hardness of LaB_6 monocrystals as 22.6 GPa and 28±0.3 GPa, respectively [41].

To the best of the authors knowledge, the fracture toughness of the bulk LaB_6 was reported only by Sonber et al. [9]. They evaluated the fracture toughness by the indentation method using a 10kg-force load. They summarized their toughness findings as 3.02±0.5 MPa $m^{1/2}$.

In this study, we evaluated the toughness by the flexural method. The average room temperature toughness of 3.2±0.3 MPa $m^{1/2}$ was observed. With an increase in the temperature we observed (see ***Fig. S1***) a decrease in toughness to the level of 1.8 MPa $m^{1/2}$ at 1200 °C. Tests at 1600 °C showed that the toughness reached a level of 1.3±0.1 MPa $m^{1/2}$, and does not depend on the specimen thermal history. It has been previously reported for the LaB_6–MeB_2 eutectics that the plasticity of LaB_6 should contribute to its strengthening [12,13]. Despite observing a plasticity on the load-displacement curves for the toughness or strength tests above 1600 °C, we observed a decrease in the strength and toughness.

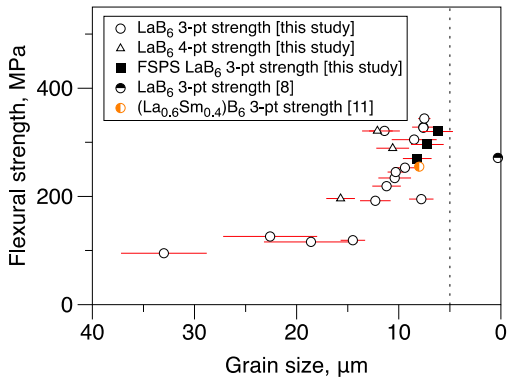

Figure 16. Effect of grain size on flexural strength for LaB_6 at room temperature. Grain size was measured for every individual bar using optical microscopy and SEM. A total of 20 bars originating from different specimens were measured. The FSPS-ed specimens are depicted as closed squares. The four-point flexural tests data are presented with an open triangles. Vertical dashed line shows the mean size of the starting powder.

The flexural strength at room temperature was reported by Zhou et al. [8] and Arabei et al. [10]. The latter study reported the strength of 126 MPa for specimens with a porosity of 3–5%, but the grain size was not reported. We summarized the results of our study for the flexural strength of the LaB_6 bulks as a function of the grain size in **Figure 16**. One can see that there is a certain Hall-Petch-like dependence on the flexural strength when the grain size changes from 8 to 20 μm. We selected two SPS conditions that yielded the highest and mean flexural strength at room temperature

to perform the high-temperature flexural tests. These attempts are summarized in **Figure 17** [12,13]. Because of a limited amount of specimens, the actual tests values are presented.

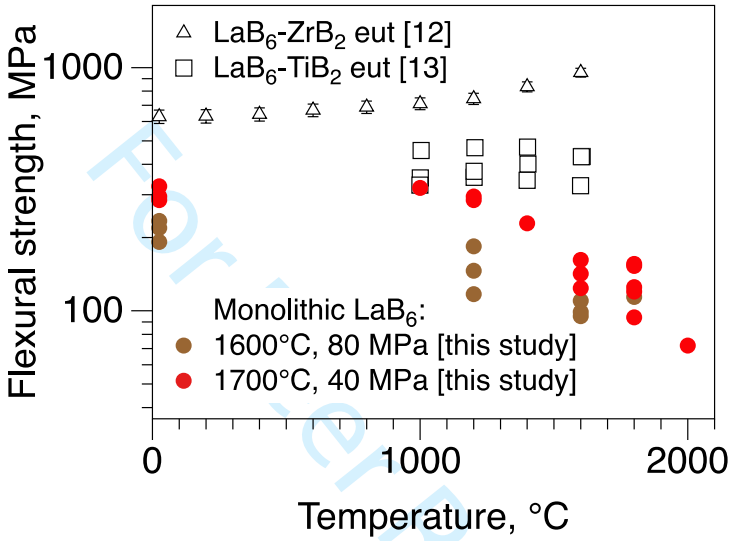

Figure 17. Effect of temperature on the flexural strength of lanthanum hexaboride and selected LaB_6-based composites [12,13].

Only the data for the LaB_6–based eutectics are available for direct comparison with the LaB_6 bulks. These studies showed either a constant increase in strength [12,13] or a slight decrease after reaching 1600 °C. In our study, we observed a slight or constant strength up to 1200 °C, while a further increase in the temperature up to 1600 °C leads to a decrease in the strength to 120±40 MPa. Tests at 1800 °C

suggested that the strength remains around the 80–120 MPa, while the single test at 2000 °C suggested that the strength further drops to 68 MPa.

The strain-stress curves (see ***Fig. S2***) suggested that the lanthanum hexaboride shows a typical plastic deformation curve. Hence, tests at 1800 °C and 2000 °C were performed using a 3 mm/min loading rate. In [12,13], it was suggested that the increase in strength can be attributed to the plasticity of the LaB_6 matrix or diboride inclusions. In the present study, we see the opposite effect; with a significant plasticity at 1600 °C, the flexural strength rapidly decreased. Fracture was mainly transgranular at the elevated temperatures (**Fig. 14**), while some large-sized grains fractured in a transgranular manner.

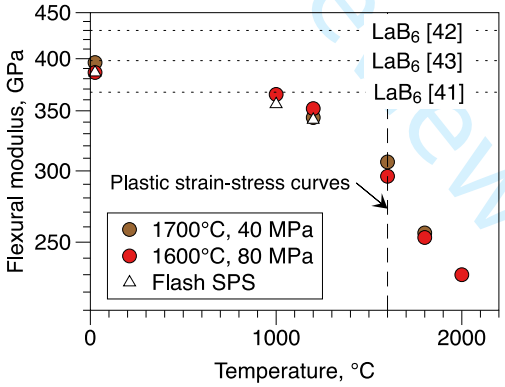

Figure 18. Effect of temperature on the flexural modulus of lanthanum hexaboride between 25 °C and 2000 °C. Horizonal dot-lines are data for polycrystalline [42] and monocrystalline [41] specimens by the nanoindentation method.

Figure 18 summarizes the flexural modulus data determined using the linear portion of the strain-stress curves, and data by Loboda et al. [41] and Wu et al. [42] from the nano-hardness. Samsonov et al. [43] reported modulus of 398 GPa for bulk LaB_6. At room temperature, we observed modulus values between 380 and 418 GPa, and, as one may expect, the elastic modulus can be approximated as a function of the porosity as E = 414.9 exp (-0.226*porosity) with the R^2 value of 0.874. With an increase in the temperature, we observed a decrease in the modulus, while after 1600 °C the decrease in the elastic modulus was more noticeable, as the values for 1800 °C are 255±6 GPa suggesting a 40% decrease in the modulus.

Considering that strength at room temperature or elastic moduli (**Figs. 16** and **18**) for the LaB_6 specimens after the SPS or FSPS are within a margin of error, one should recall that the FSPS processing may offer a significant time or energy savings [18]. Obviously, one cannot ignore the coarse grains on the overheated side of the FSPSed specimen (such as in **Figs. 8** or **9**). We may only suggest to remove such an area by grinding if the LaB_6 specimen with a homogenous grain size is required.

Conclusions

In summary, we show that lanthanum hexaboride bulks can be consolidated to their theoretical density consolidated using spark-plasma sintering while using a relatively short dwell time. An alternative method of direct heating a porous sample

using SPS in the flash regime allows to further decrease the time of consolidation within hundreds of seconds. The flash spark plasma sintering process is accompanied by local coarsening of the LaB_6 to 200–300 μm, which is believed to be a direct consequence of the self-heating of the ceramic, including the possibility of local electron plasma ignition. Isothermal kinetics using regular SPS allowed us to determine the activation energy for sintering as 150±30 kJ/mol.

This is the first study to show the high-temperature strength or toughness of LaB_6. The bulk LaB_6 was shown to have a relatively low fracture toughness of 3.2±0.3 MPa $m^{1/2}$ at room temperature and relatively high hardness of 16.3±0.4GPa. The flexural strength had a Hall-Petch-like dependence on the grain size and varied from 90 MPa to 330 MPa. With an increase in the temperature, both the toughness and strength showed a gradual decrease to 1.3±0.1 MPa $m^{1/2}$ and 120±40 MPa at 1600 °C, respectively. Above 1600 °C, we observed a plastic-like deviation on the strain-stress curves suggesting that initiation of the plastic deformation leads to a decrease in the strength, toughness and elastic modulus.

Acknowledgements

Authors express their sincere appreciation to Dr. Toshiyuki Nishimura (NIMS) for providing access to the evaluation of high-temperature strength, this study would not be as complete otherwise. D.D. expresses his gratitude to Dr. Byung-Nam Kim

(NIMS) for his comments on the structure evolution during the flash spark plasma sintering.

References

[1] Samsonov GV. Refractory Compounds of Rare-Earth Metals with Nonmetals. Moscow: Metallurgiya; 1964. [in Russian]

[2] Samsonov GV, Paderno YuB. Borides of the Rare-Earth Metals. Kiev: Acad. Sci. Ukr. SSR Press; 1961. [in Russian]

[3] Kunitskii Yu A, Morozov VV, Shlyuko V Ya. High-Temperature Electrode Materials. Kiev: Vishcha Shkola; 1977. [in Russian]

[4] Lafferty JM. Boride cathodes. J. Appl. Phys. 1951;22:299–309. https://doi.org/10.1063/1.1699946.

[5] Samsonov GV, Vinitsky IM. Refractory Compounds. Handbook; Moscow: Metallurgiya; 1976. [in Russian]

[6] Sani E, Mercatelli L, Meucci M, Zoli L, Sciti D. Lanthanum hexaboride for solar energy applications. Sci. Rep. 2017;7:718. https://doi.org/10.1038/s41598-017-00749-w.

[7] Andrievski RA, Spivak II. Strength of Refractory Compounds; Chelyabinsk: Metallurgiya; 1989. [in Russian]

[8] Zhou S, Zhang J, Liu D, Lin Z, Huang Q, Bao L, Ma R, Wei Y. Synthesis and properties of nanostructured dense LaB6 cathodes by arc plasma and reactive spark plasma sintering. Acta Mater. 2010;58(15):4978–4985. https://doi.org/10.1016/j.actamat.2010.05.031.

[9] Sonber JK, Sariam K, Murthy TSRCh, Nagaraj A, Subramanian C, Hubli RC. Synthesis, densification and oxidation study of lanthanum hexaboride. J. Eur. Ceram. Soc. 2014;34(5):1155–1160. https://doi.org/10.1016/j.jeurceramsoc.2013.11.023.

[10] Arabei BG, Shtrom EN, Lapitskii YA. Characteristics of the manufacturing technology of dense parts from, and the mechanical properties of, some hexaborides of the rare-earth metals. Powder Metall. Met. Ceram. 1965;3:406–409. https://doi.org/10.1007/BF00774242.

[11] Zhou S, Zhang J., Liu D, Hu Q, Huang Q. The effect of samarium doping on structure and enhanced thermionic emission properties of lanthanum hexaboride fabricated by spark plasma sintering. Phys. Status Solidi. 2014;211(3):555–564. https://doi.org/10.1002/pssa.201330152.

[12] Bogomol I, Nishimura T, Nestrerenko Yu, Vasylkiv O, Sakka Y, Loboda P. The bending strength temperature dependence of the directionally solidified eutectic LaB6–ZrB2 composite. J. Alloys Compd. 2011;509(20):6123–6129. https://doi.org/10.1016/j.jallcom.2011.02.176.

[13] Bogomol I, Nishimura T, Vasylkiv O, Sakka Y, Loboda P. High-temperature strength of directionally reinforced LaB6–TiB2 composite. J. Alloys Compd. 2010;505(1):130–134. https://doi.org/10.1016/j.jallcom.2010.05.003.

[14] Chaill JT, Greave OA, Hexaborides: a review of structure, synthesis and processing. J. Mater. Res. Technol. 2019;8(6):6321–6335. https://doi.org/10.1016/j.jmrt.2019.09.041.

[15] Tanaka T. The thermal and electrical conductivities of LaB6 at high temperatures. J. Phys. C: Solid State Phys. 1974;7:L177–L180. https://doi.org/10.1088/0022-3719/7/9/001.

[16] Williams MD, Jackson LT, Kippenhan DO, Leung KN, West MK. Lanthanum hexaboride (LaB6) resistivity measurement. Appl. Phys. Lett. 1987;50:1844–1845. https://doi.org/10.1063/1.97715.

[17] Cooper CM, Gekelman W, Pribyl P, Lucky Z. A new large area lanthanum hexaboride plasma source. Rev. Sci. Instrum. 2010;81:083503. https://doi.org/10.1063/1.3471917.

[18] Yu M, Grasso S, Mckinnon R, Saunders T, Reece MJ. Review of flash sintering: materials, mechanisms and modelling. Adv. Appl. Ceram. 2017;116(1):24–60. https://doi.org/10.1080/17436753.2016.1251051.

[19] Vasylkiv O, Bordianska H, Sakka Y, Demirskyi D. Flash spark plasma sintering of ultrafine yttria-stabilized zirconia ceramics. Scr. Mater. 2016;121:32–36. https://doi.org/10.1016/j.scriptamat.2016.04.031.

[20] Demirskyi D, Vasylkiv O. Hot-spots generation, exaggerated grain growth and mechanical performance of silicon carbide bulks consolidated by flash spark plasma sintering. J. Alloys Compd. 2017;691:466–473. https://doi.org/10.1016/j.jallcom.2016.08.234.

[21] Demirskyi D, Suzuki TS, Grasso S, Vasylkiv O. Microstructure and flexural strength of hafnium diboride via flash and conventional spark plasma sintering. J. Eur. Ceram. Soc. 2019;39(4):898–906. https://doi.org/10.1016/j.jeurceramsoc.2018.12.012

[22] Demirskyi D, Vasylkiv O. Consolidation and grain growth of tantalum diboride during spark plasma sintering. Ceram. Int. 2016;42(14):16396–16400. https://doi.org/10.1016/j.ceramint.2016.07.059.

[23] Vasylkiv O, Demirskyi D, Borodianska H, Sakka Y, Badica P. High temperature flexural strength in monolithic boron carbide ceramic obtained from two different raw powders by spark plasma sintering. J Ceram. Soc. Japan. 2016;124(5):587–592. https://doi.org/10.2109/jcersj2.15289.

[24] Demirskyi D, Vasylkiv O. Analysis of the high-temperature flexural strength behavior of B4C–TaB2 eutectic composites produced by in situ spark plasma

sintering. Mater. Sci. Eng. A. 2017;697:71–78. https://doi.org/10.1016/j.msea.2017.04.093.

[25] Demirskyi D, Vasylkiv O. Spark plasma sintering and high-temperature strength of B6O–TaB2 ceramics. J. Eur. Ceram. Soc. 2017;37(8):3009–3014. https://doi.org/10.1016/j.jeurceramsoc.2017.02.052.

[26] Murray P, Rodgers EP, Williams AE. Practical and theoretical aspects of the hot pressing of refractory oxides. Trans. Brit. Ceram. Soc. 1954;53:474–510.

[27] Thumler F, Thomma W. The sintering process. Met. Review. 1969;12(1): 69–108. https://doi.org/10.1179/mtlr.1967.12.1.69.

[28] Mangsen GE, Lamberson WA, Best B. Hot Pressing of Aluminum Oxide. J. Am. Ceram. Soc. 1960;43(2):55–59. https://doi.org/10.1111/j.1151-2916.1960.tb13640.x.

[29] Vasilos T. Hot Pressing of Fused Silica. J. Am. Ceram. Soc. 1960;43(10):517–519. https://doi.org/10.1111/j.1151-2916.1960.tb13606.x.

[30] Jaeger RE, Egerton L. Hot Pressing of Potassium-Sodium Niobates. J. Am. Ceram. Soc. 1962;45(5):209–213. https://doi.org/10.1111/j.1151-2916.1962.tb11127.x.

[31] Samsonov GV, Koval'chenko MS. Hot Pressing. Kiev: Gostekhizdat USSR; 1962. [in Russian].

[32] Topor L, Kleppa OJ. Standard molar enthalpy of formation of LaB6 by high-temperature calorimetry. J. Chem. Thermodyn. 1984;16(10):993–1002. https://doi.org/10.1016/0021-9614(84)90169-1.

[33] Paradis P-F, Ishikawa T, Koike N, Watanabe Y. Study of Molten Lanthanum, Praseodymium, and Neodymium by Electrostatic Levitation. Int. J. Microgravity Sci. Appl. 2008;25(3):407. https://doi.org/10.15011/jasma.25.3.407.

[34] Paradis P-F, Ishikawa T, Yoda S. Surface tension and viscosity of liquid and undercooled tantalum measured by a containerless method. J. Appl. Phys. 2005;97:053506. https://doi.org/10.1063/1.1854211.

[35] Doremus RH. Glass Science. 2nd Ed. New York, NY US: John Wiley & Sons Inc.; 1994.

[35] Raichenko AI. Fundamentals of Sintering of Powders by Passing an Electric Current. Moscow: Metallurgiya; 1987. [in Russian]

[36] Schneider CA, Rasband WS, Eliceiri KW. NIH Image to ImageJ: 25 years of image analysis. Nat. Methods. 2012;9(7):671–675.

[37] Demirskyi D, Borodianska H, Grasso S, Sakka Y, Vasylkiv O. Microstructure evolution during field-assisted sintering of zirconia spheres. Scr. Mater. 2011;65(8):683–686. https://doi.org/10.1016/j.scriptamat.2011.07.006.

[38] Kotelnikov RB, Bashlikov SN, Galiakbarov SG, Kashtanov AI. High Melting-Point Compounds. A Companion. Moscow: Metallurgyia; 1969. [in Russian]

[39] Korsukova MM, Gurin VN. Physicochemical Problems in the Preparation of Defect-free Monocrystals of Lanthanum Hexaboride. Russ. Chem. Rev. 1987;56(1):1–15. https://doi.org/10.1070/RC1987v056n01ABEH003252.

[40] Otani S, Tanaka T, Ishizawa Y. Crystal quality and high temperature hardness of LaB6 crystals prepared by the floating zone method. J. Alloys Compd. 1993;202(1–2):L25–L28. https://doi.org/10.1016/0925-8388(93)90506-I.

[41] Loboda PI, Kysla HP, Dub SM, Karasevs'ka OP. Mechanical properties of the monocrystals of lanthanum hexaboride. Mater. Sci. 2009;45:108–113. https://doi.org/10.1007/s11003-009-9167-6.

[42] Wu X, Xu TT. Measurement of mechanical properties of alkaline-earth metal hexaboride one-dimensional nanostructures by nanoindentation. J. Mater. Res. 2012;27(9):1218–1229. https://doi.org/10.1557/jmr.2012.82

[43] Samsonov GV, Koval'chenko MS, Ogorodnykov VV, Krainiy AG. Investigation on radiation stability of borides. Atomic Energy. 1968;24:232–233. https://doi.org/10.1007/BF01114199.

Figure caption

Figure 1. Effect of temperature and dwell on relative density the LaB_6 using the constant pressure of (a) 40 MPa, (b) 60 MPa, and (c) 80 MPa.

Figure 2. Relationship between logarithm of porosity and time for LaB_6 compacts SPSed at various temperatures using the constant pressure of (a) 40 MPa, (b) 60 MPa, and (c) 80 MPa.

Figure 3. Arrhenius dependence of logarithm of viscosity evaluated for LaB_6 during spark plasma sintering using the constant pressures of 40, 60, and 80 MPa.

Figure 4. Effect of temperature on the evaluated viscosity of the LaB_6 using different pressures.

Figure 5. Grain size as a function of the relative density during isothermal dwell runs using spark plasma sintering. We present the temperature for the isothermal dwell in the case of extremely coarse grains.

Figure 6. Variation in shrinkage, temperature, current and voltage during flash SPS of LaB_6. Note the quasi-linear dependance between the temperature and current. The maximum current was fixed at (a) 3000 A, (b) 2000 A, and (c) 2700 A. The horizontal lines are for the reference specimens stopped during heating that were used to understand the microstructure evolution.

Figure 7. Representative microstructures of lanthanum hexaboride consolidated using flash SPS at different locations on the specimen. Flash SPS process was

stopped after reaching ~1300±20°C (see specimen 3 in **Fig. 6 (c)**). Current flow is from the bottom to top. Images are taken in the BSE mode. The 20–25 μm thick tantalum carbide layer that originated from the green-specimen processing can be seen as a white continuous strip. No reaction between Ta or TaC with LaB_6 was noticed during processing. The thickness of the green specimen was approximately 10 mm, and at an ~500 μm distance from the top surface a more dense microstructure was observed. The mean grain size was unchanged at 5±1 μm. The black areas are pores or dirt introduced during polishing of the specimen.

Figure 8. Representative microstructures of lanthanum hexaboride consolidated using flash SPS at different locations on the specimen. The flash SPS process was stopped after reaching ~1410±10°C. Current flow is from the top to bottom as indicated by the arrow in (a). Macroscopic images are taken in the BSE mode. The thickness of the green specimen was 8 mm. The black areas in (j) are pores or pull-outs introduced during polishing of the specimen.

Figure 9. Representative microstructures of lanthanum hexaboride consolidated using flash SPS at 1480±10°C at different locations on the specimen. Internal SEM numbering was used. This is a half-bar after the flexural test to determine the fracture toughness at room temperature.

Figure 10. Mean grain size and total porosity for lanthanum hexaboride consolidated using flash SPS at different locations on the specimen. Numbers are the same as in

Fig 9. (b) and (c) show the histograms for the pore-size distribution at different ends of the specimen.

Figure 11. Representative microstructure of lanthanum hexaboride consolidated using flash SPS at ~1500±10°C. Current flow is from the top to bottom. The thickness of the green specimen was 5 mm. (a) image is taken in the BSE mode. (b) image shows the algorithm for evaluation of the grain size using a self-learning engine. (c) provides a grain size distribution for the specimen. The black areas in (a) and (b) are grain pullouts during polishing or voids associated with fast grain-growth and related accommodation in the enclosed volume.

Figure 12. Representative microstructures of lanthanum hexaboride consolidated using flash SPS at ~1500±20°C. Current flow is from the bottom to top. The thickness of the green specimen was 6 mm. (a2) image is taken in the BSE mode. The 30-μm thick tantalum carbide foil originated from the green-specimen processing can be seen as a white continuous strip in (a2). Right side shows grain size distribution for SEM images observed 300 μm from each other. Relative density of the specimen was 98.7±0.2% of the theoretical density.

Figure 13. Diffraction pattern of the lanthanum hexaboride specimen (a) before FSPS, and (b) after FSPS.

Figure 14. Representative microstructures of lanthanum hexaboride consolidated using SPS at 1700 °C and pressure of 40 MPa. (a,d) polished surface, black areas in

(d) are pores and pull-out grains. (b,e) and (c,f) are fractured at 1600 °C and 1800 °C, respectively.

Figure 15. Representative microstructures of lanthanum hexaboride consolidated using SPS at 2000 °C and pressure of 50 MPa. Specimens were heated and cooled at the rate of 100°C/min. Dwell was not used. (a) is for the specimen center, while (b) was observed at the specimen edge. In both cases, the top polished surface was used. Images are taken in the BSE mode. (c) and (d) show typical grain-boundary shape using the self-learning engine. (c) for the SPS at 2000°C using (a); and (d) for the FSPS (**Fig. 8 (d)**) using identical magnification.

Figure 16. Effect of grain size on flexural strength for LaB_6 at room temperature. Grain size was measured for every individual bar using optical microscopy and SEM. A total of 20 bars originating from different specimens were measured. The FSPS-ed specimens are depicted as closed squares. The four-point flexural tests data are presented with an open triangles. Vertical dashed line shows the mean size of the starting powder.

Figure 17. Effect of temperature on the flexural strength of lanthanum hexaboride and selected LaB_6-based composites [12,13].

Figure 18. Effect of temperature on the flexural modulus of lanthanum hexaboride between 25 °C and 2000 °C. Horizonal dot-lines are data for polycrystalline [42] and monocrystalline [41] specimens by the nanoindentation method.

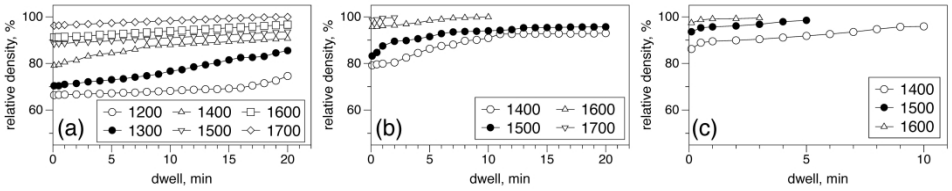

Figure 1. Effect of temperature and dwell on relative density the LaB_6 using the constant pressure of (a) 40 MPa, (b) 60 MPa, and (c) 80 MPa.

386x81mm (300 x 300 DPI)

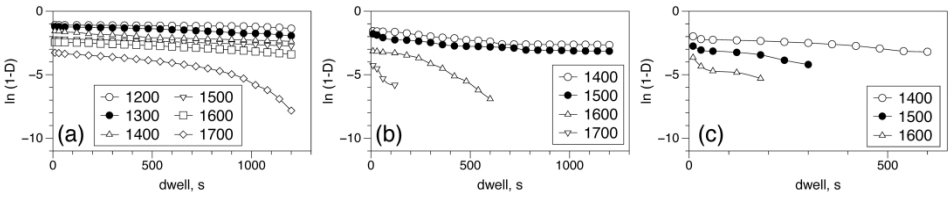

Figure 2. Relationship between logarithm of porosity and time for LaB_6 compacts SPSed at various temperatures using the constant pressure of (a) 40 MPa, (b) 60 MPa, and (c) 80 MPa.

386x81mm (300 x 300 DPI)

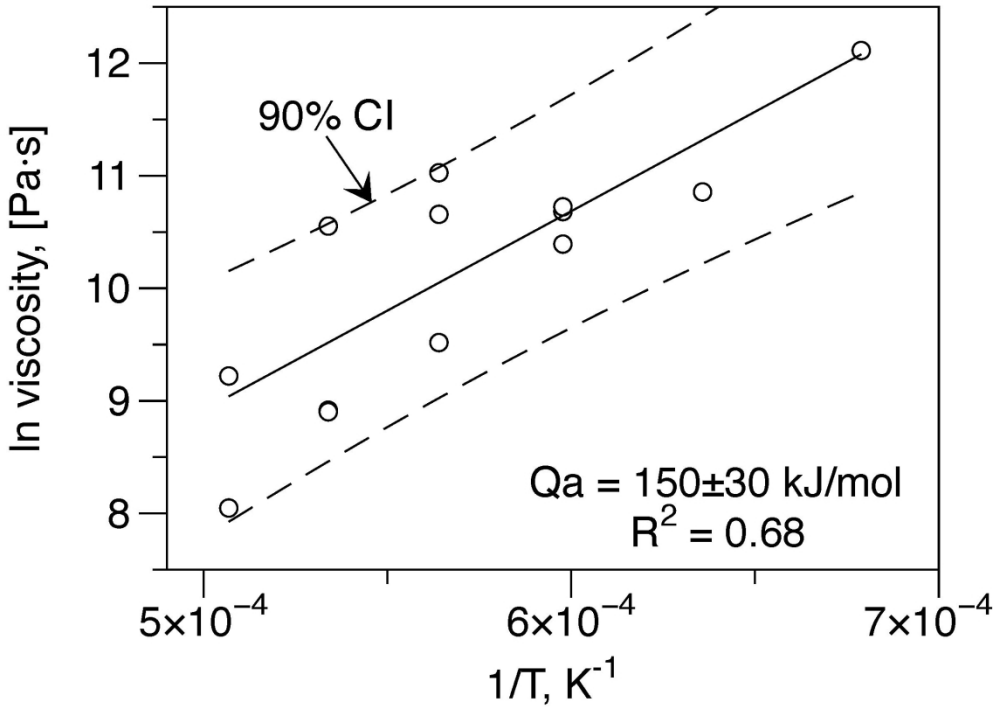

Figure 3. Arrhenius dependence of logarithm of viscosity evaluated for LaB_6 during spark plasma sintering using the constant pressures of 40, 60, and 80 MPa.

101x76mm (600 x 600 DPI)

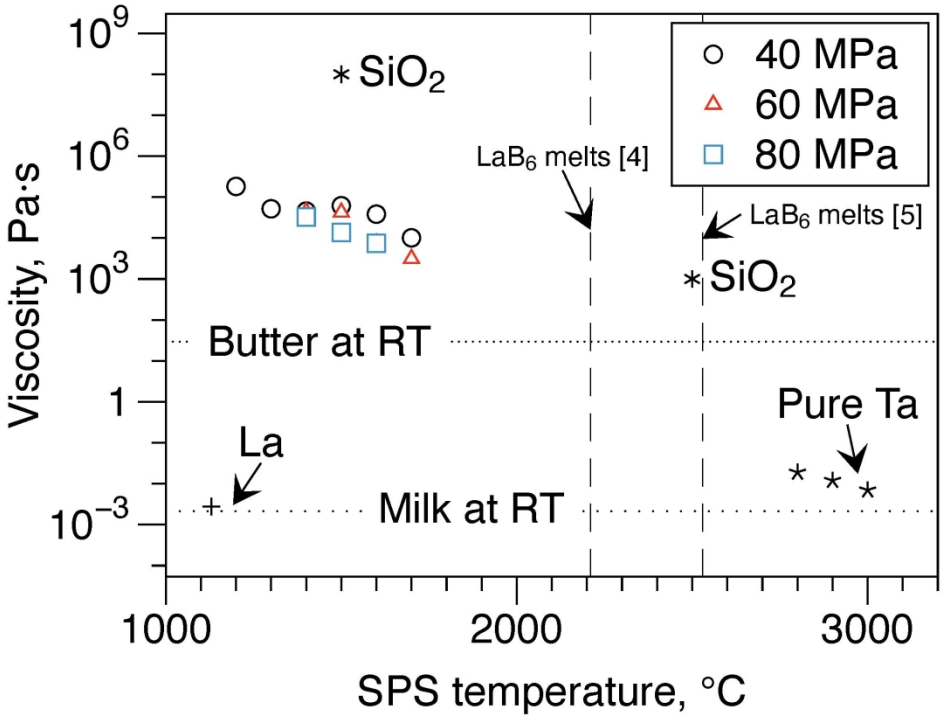

Figure 4. Effect of temperature on the evaluated viscosity of the LaB_6 using different pressures.

101x76mm (600 x 600 DPI)

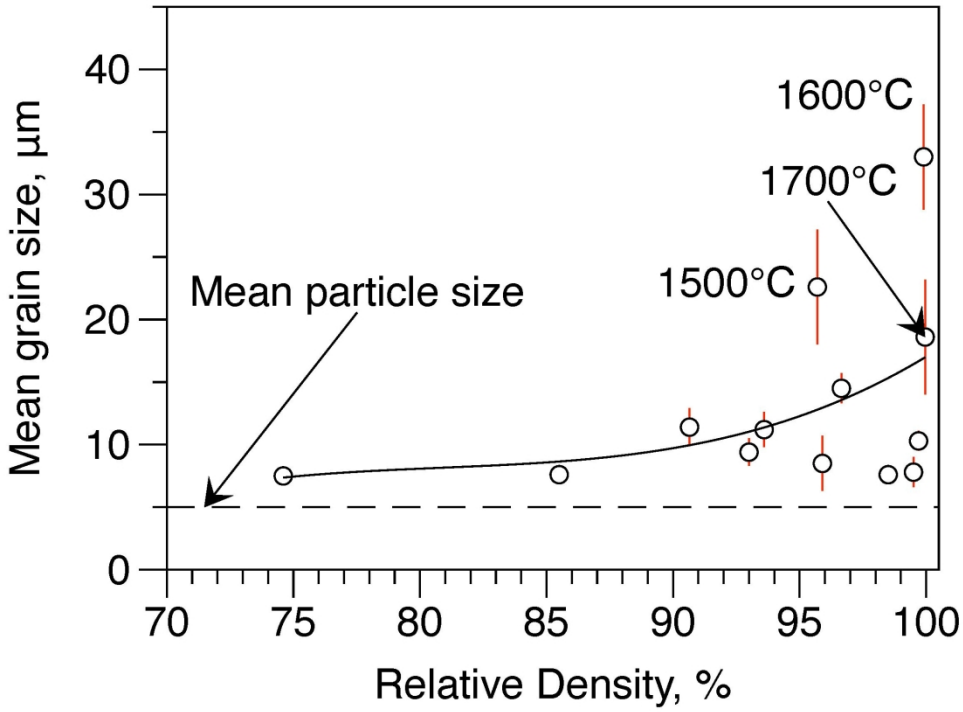

Figure 5. Grain size as a function of the relative density during isothermal dwell runs using spark plasma sintering. We present the temperature for the isothermal dwell in the case of extremely coarse grains.

101x76mm (600 x 600 DPI)

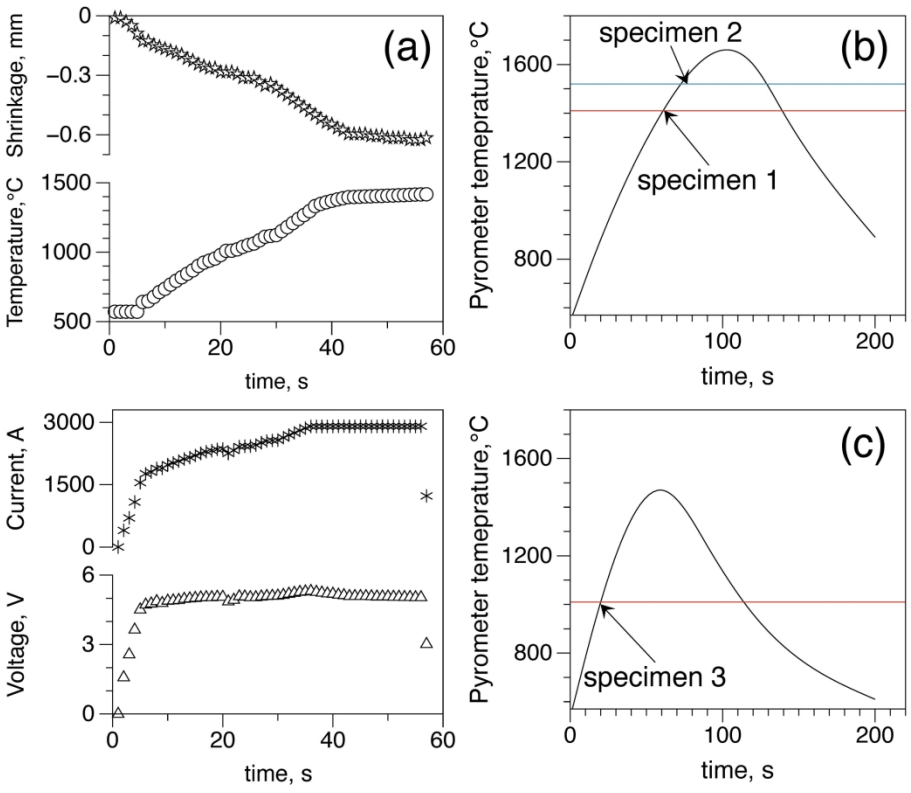

Figure 6. Variation in shrinkage, temperature, current and voltage during flash SPS of LaB_6. Note the quasi-linear dependance between the temperature and current. The maximum current was fixed at (a) 3000 A, (b) 2000 A, and (c) 2700 A. The horizontal lines are for the reference specimens stopped during heating that were used to understand the microstructure evolution.

213x177mm (300 x 300 DPI)

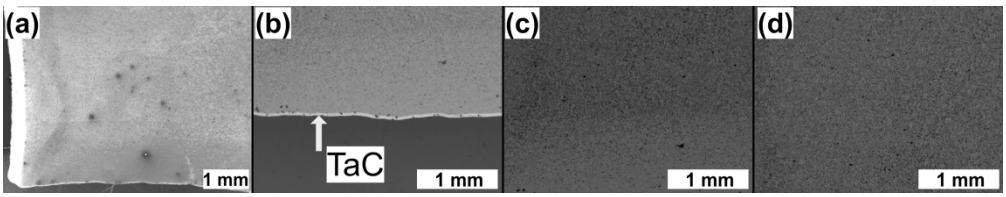

Figure 7. Representative microstructures of lanthanum hexaboride consolidated using flash SPS at different locations on the specimen. Flash SPS process was stopped after reaching ~1300±20°C (see specimen 3 in **Fig. 6 (c)**). Current flow is from the bottom to top. Images are taken in the BSE mode. The 20–25 μm thick tantalum carbide layer that originated from the green-specimen processing can be seen as a white continuous strip. No reaction between Ta or TaC with LaB_6 was noticed during processing. The thickness of the green specimen was approximately 10 mm, and at an ~500 μm distance from the top surface a more dense microstructure was observed. The mean grain size was unchanged at 5±1 μm. The black areas are pores or dirt introduced during polishing of the specimen.

326x60mm (300 x 300 DPI)

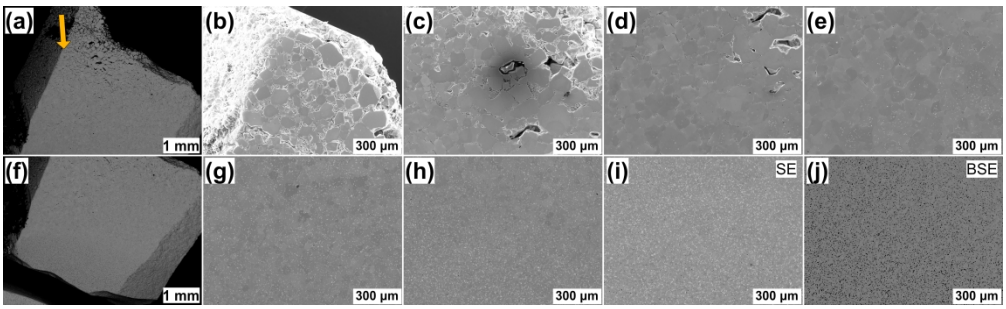

Figure 8. Representative microstructures of lanthanum hexaboride consolidated using flash SPS at different locations on the specimen. The flash SPS process was stopped after reaching ~1410±10°C. Current flow is from the top to bottom as indicated by the arrow in (a). Macroscopic images are taken in the BSE mode. The thickness of the green specimen was 8 mm. The black areas in (j) are pores or pull-outs introduced during polishing of the specimen.

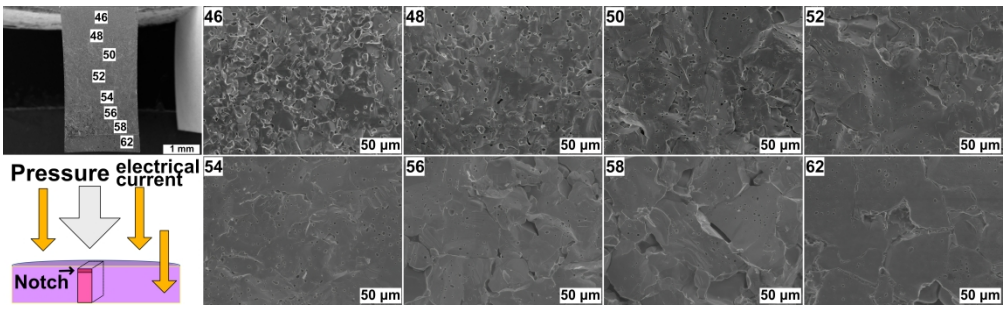

Figure 9. Representative microstructures of lanthanum hexaboride consolidated using flash SPS at 1480±10°C at different locations on the specimen. Internal SEM numbering was used. This is a half-bar after the flexural test to determine the fracture toughness at room temperature.

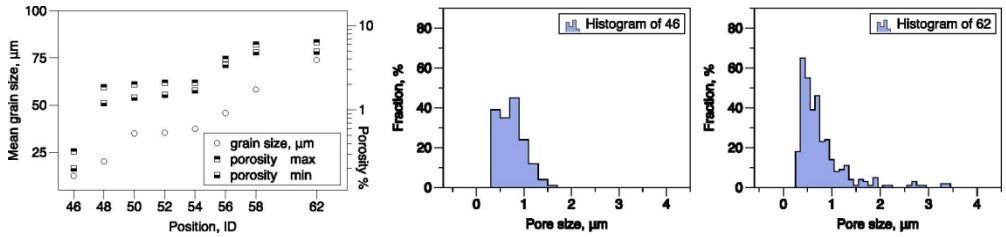

Figure 10. Mean grain size and total porosity for lanthanum hexaboride consolidated using flash SPS at different locations on the specimen. Numbers are the same as in **Fig 9. (b)** and **(c)** show the histograms for the pore-size distribution at different ends of the specimen.

76x17mm (600 x 600 DPI)

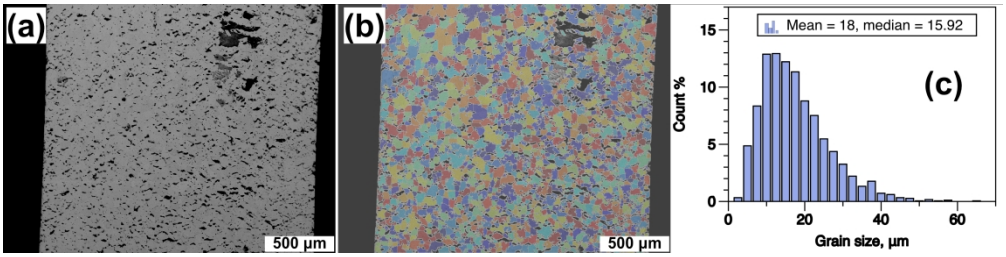

Figure 11. Representative microstructure of lanthanum hexaboride consolidated using flash SPS at ~1500±10°C. Current flow is from the top to bottom. The thickness of the green specimen was 5 mm. (a) image is taken in the BSE mode. (b) image shows the algorithm for evaluation of the grain size using a self-learning engine. (c) provides a grain size distribution for the specimen. The black areas in (a) and (b) are grain pullouts during polishing or voids associated with fast grain-growth and related accommodation in the enclosed volume.

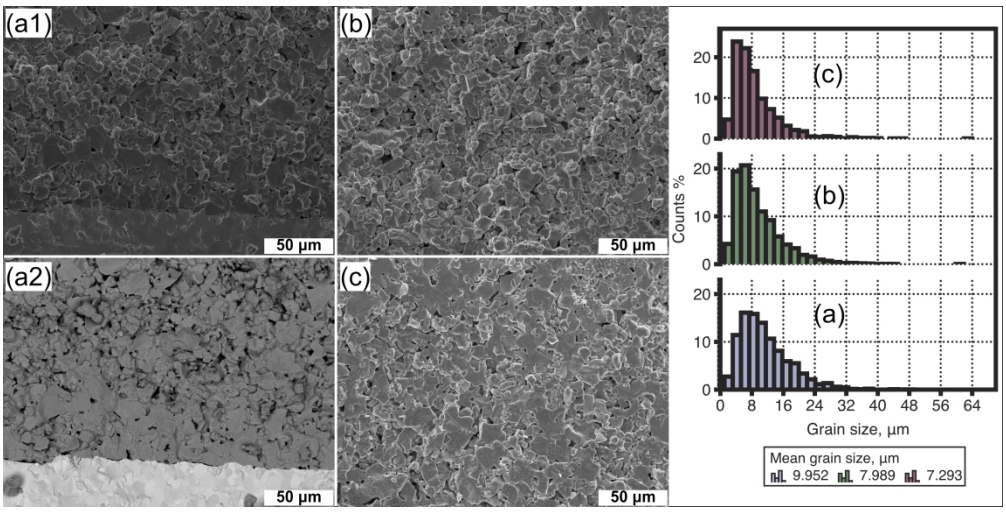

Figure 12. Representative microstructures of lanthanum hexaboride consolidated using flash SPS at ~1500±20°C. Current flow is from the bottom to top. The thickness of the green specimen was 6 mm. (a2) image is taken in the BSE mode. The 30-μm thick tantalum carbide foil originated from the green-specimen processing can be seen as a white continuous strip in (a2). Right side shows grain size distribution for SEM images observed 300 μm from each other. Relative density of the specimen was 98.7±0.2% of the theoretical density.

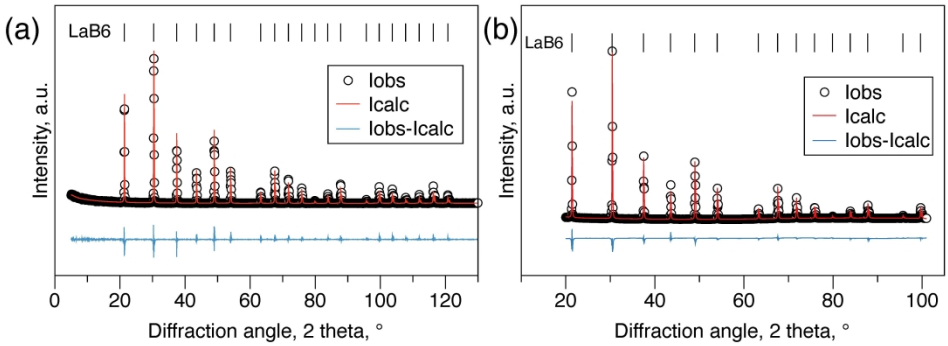

Figure 13. Diffraction pattern of the lanthanum hexaboride specimen (a) before FSPS, and (b) after FSPS.

211x81mm (600 x 600 DPI)

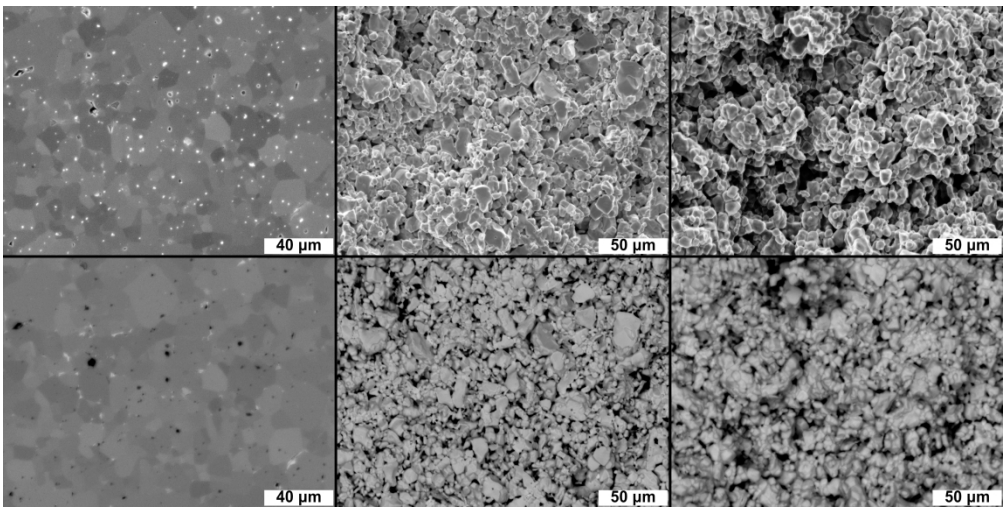

Figure 14. Representative microstructures of lanthanum hexaboride consolidated using SPS at 1700°C and pressure of 40 MPa. (a,d) polished surface, black areas in (d) are pores and pull-out grains. (b,e) and (c,f) are fractured at 1600°C and 1800°C, respectively.

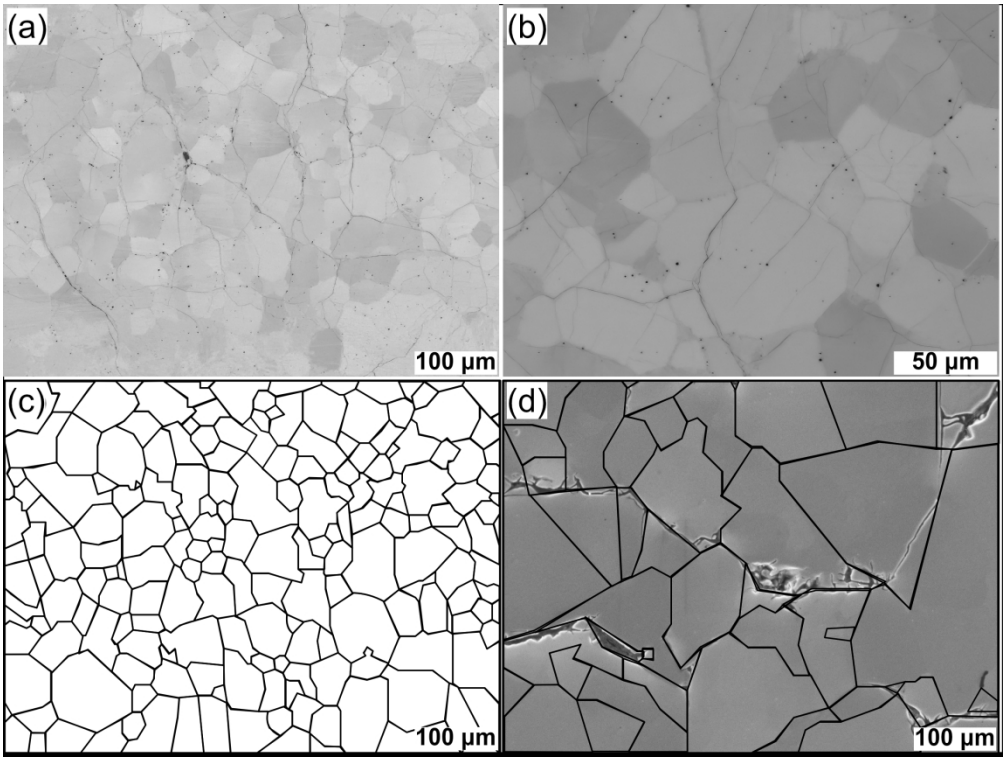

Figure 15. Representative microstructures of lanthanum hexaboride consolidated using SPS at 2000°C and pressure of 50 MPa. Specimens were heated and cooled at the rate of 100°C/min. Dwell was not used. (a) is for the specimen center, while (b) was observed at the specimen edge. In both cases, the top polished surface was used. Images are taken in the BSE mode. (c) and (d) show typical grain-boundary shape using the self-learning engine. (c) for the SPS at 2000°C using (a); and (d) for the FSPS (**Fig. 8 (d)**) using identical magnification.

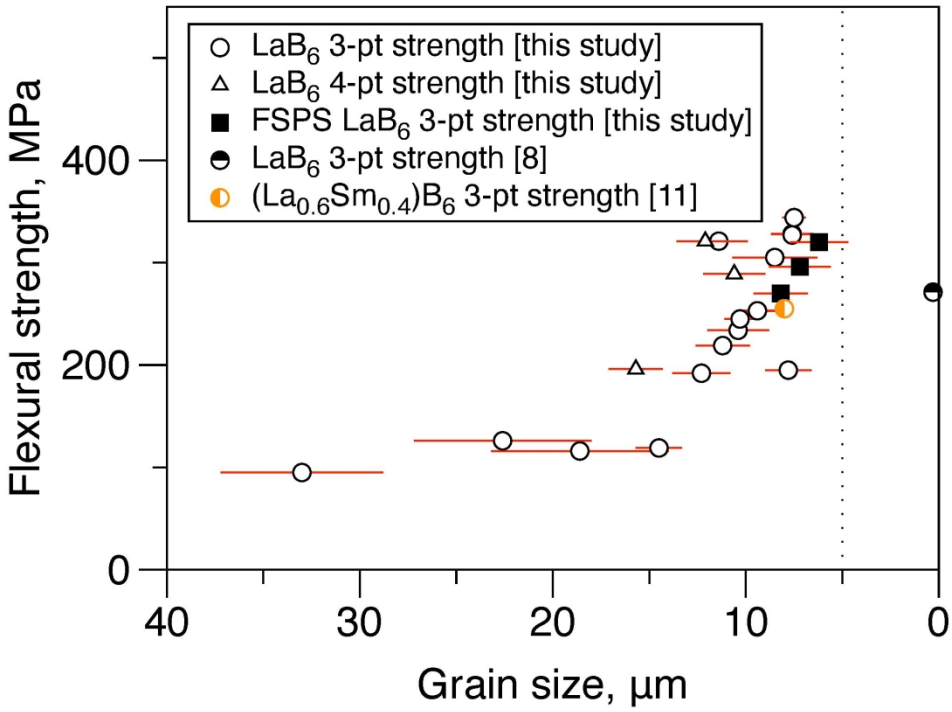

Figure 16. Effect of grain size on flexural strength for LaB_6 at room temperature. Grain size was measured for every individual bar using optical microscopy and SEM. A total of 20 bars originating from different specimens were measured. The FSPS-ed specimens are depicted as closed squares. The four-point flexural tests data are presented with an open triangles. Vertical dashed line shows the mean size of the starting powder.

101x76mm (600 x 600 DPI)

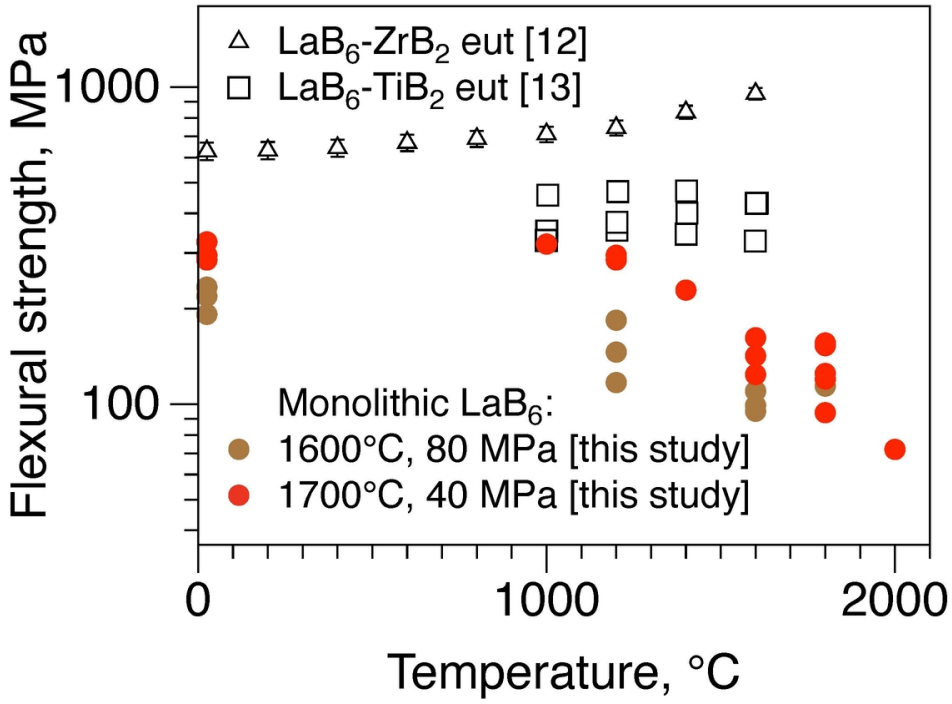

Figure 17. Effect of temperature on the flexural strength of lanthanum hexaboride and selected LaB_6-based composites [12,13].

101x76mm (300 x 300 DPI)

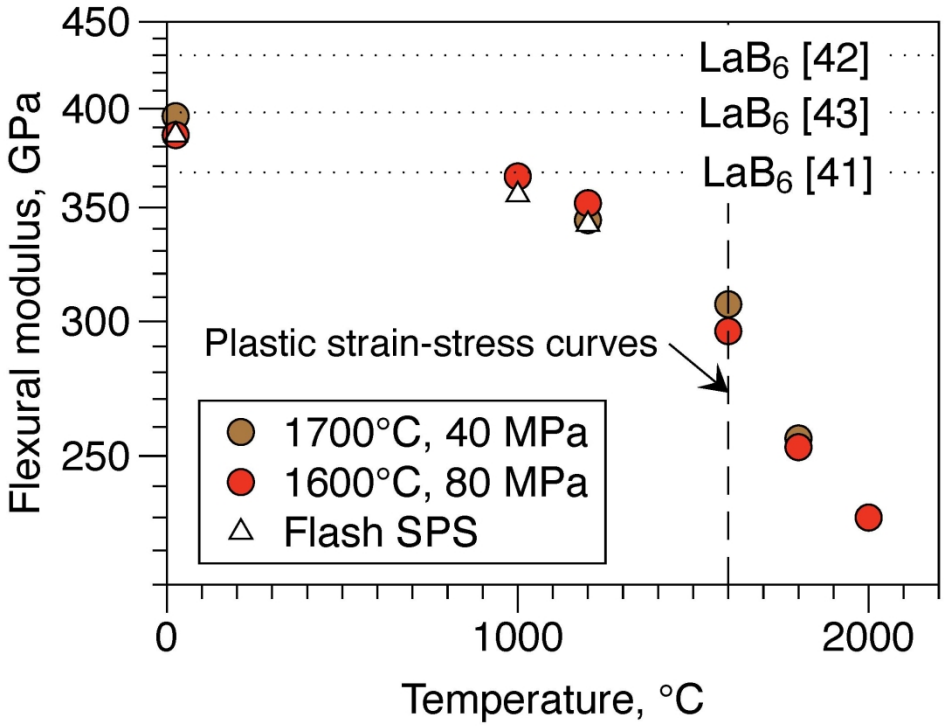

Figure 18. Effect of temperature on the flexural modulus of lanthanum hexaboride between 25°C and 2000°C. Horizonal dot-lines are data for polycrystalline [42] and monocrystalline [41] specimens by the nanoindentation method.

101x76mm (600 x 600 DPI)

Consolidation and high-temperature strength of monolithic lanthanum hexaboride

D. Demirskyi (a,b,c)†, T.S. Suzuki (b), K. Yoshimi (c), O. Vasylkiv (b)†.

(a) WPI-Advanced Institute for Materials Research (WPI-AIMR), Tohoku University, 2-1-1 Katahira, Aoba-ku, Sendai, 980-8577 Japan
(b) National Institute for Materials Science, 1-2-1 Sengen, Tsukuba, Ibaraki 305-0047, Japan
(c) Department of Materials Science and Engineering, Tohoku University, 6-6-02 Aramaki Aza Aoba, Sendai, 980-8579, Japan

Supplementary data.

In this appendix, the typical loading curves obtained during flexural tests in LaB_6 ceramics will be presented.

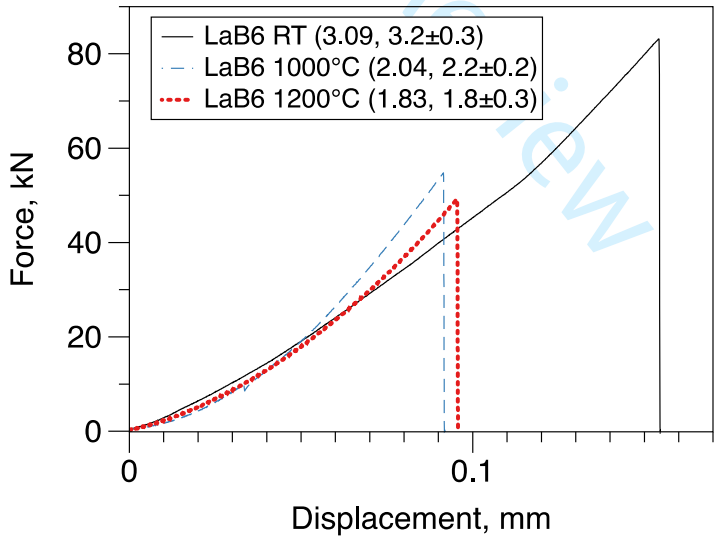

Figure S1. Effect of temperature on the fracture toughness of lanthanum hexaboride between 25 °C and 1200 °C. Numbers in brackets are the fracture toughness values

for presented curves followed by a mean value with a standard deviation observed for all attempted specimens at this temperature.

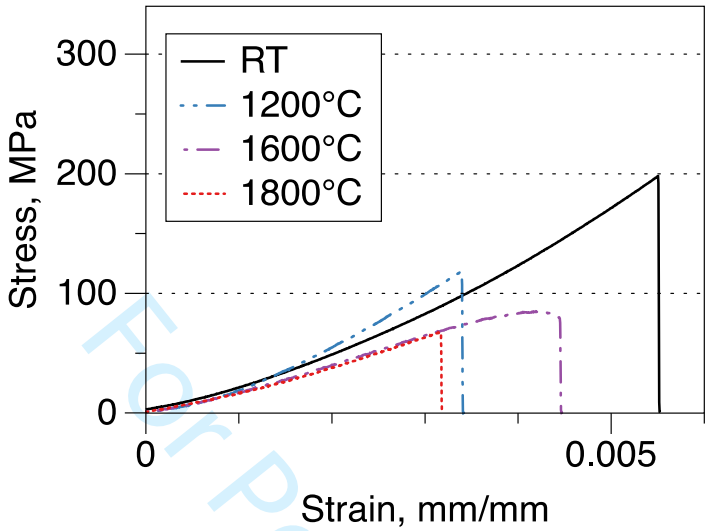

Figure S2. Typical strain-stress curves of lanthanum hexaboride bulks at different temperatures. For 1800 °C, the 3 mm/min loading rate was used, while the other tests were performed using a loading rate of 0.5 mm/min.